nature biomedical engineering

ARTICLES

https://doi.org/10.1038/s41551-019-0497-x

Robotic fluidic coupling and interrogation of multiple vascularized organ chips

Richard Novak[1,13], Miles Ingram[1], Susan Marquez[1], Debarun Das[2,13], Aaron Delahanty[1], Anna Herland[1,10,13], Ben M. Maoz[1,3,11,13], Sauveur S. F. Jeanty[1,12], Mahadevabharath R. Somayaji[2,13], Morgan Burt[1], Elizabeth Calamari[1], Angeliki Chalkiadaki[1], Alexander Cho[2], Youngjae Choe[1], David Benson Chou[1,4], Michael Cronce[1], Stephanie Dauth[1,3], Toni Divic[1], Jose Fernandez-Alcon[1,12], Thomas Ferrante[1], John Ferrier[1,3], Edward A. FitzGerald[1], Rachel Fleming[1], Sasan Jalili-Firoozinezhad[1,5], Thomas Grevesse[1,3], Josue A. Goss[1,3], Tiama Hamkins-Indik[1], Olivier Henry[1], Chris Hinojosa[1,12], Tessa Huffstater[1], Kyung-Jin Jang[1,12], Ville Kujala[1,3,12], Lian Leng[1,12], Robert Mannix[1,6], Yuka Milton[1], Janna Nawroth[1,3,12], Bret A. Nestor[1], Carlos F. Ng[1], Blakely O'Connor[1,3], Tae-Eun Park[1], Henry Sanchez[1], Josiah Sliz[1,12], Alexandra Sontheimer-Phelps[1,7], Ben Swenor[1], Guy Thompson II[1,12], George J. Touloumes[1,3], Zachary Tranchemontagne[1], Norman Wen[1,12], Moran Yadid[1,3], Anthony Bahinski[1,8], Geraldine A. Hamilton[1,12], Daniel Levner[1,12], Oren Levy[1], Andrzej Przekwas[2], Rachelle Prantil-Baun[1,13], Kevin K. Parker[1,3] and Donald E. Ingber[1,6,9*]

Organ chips can recapitulate organ-level (patho)physiology, yet pharmacokinetic and pharmacodynamic analyses require multi-organ systems linked by vascular perfusion. Here, we describe an 'interrogator' that employs liquid-handling robotics, custom software and an integrated mobile microscope for the automated culture, perfusion, medium addition, fluidic linking, sample collection and in situ microscopy imaging of up to ten organ chips inside a standard tissue-culture incubator. The robotic interrogator maintained the viability and organ-specific functions of eight vascularized, two-channel organ chips (intestine, liver, kidney, heart, lung, skin, blood–brain barrier and brain) for 3 weeks in culture when intermittently fluidically coupled via a common blood substitute through their reservoirs of medium and endothelium-lined vascular channels. We used the robotic interrogator and a physiological multicompartmental reduced-order model of the experimental system to quantitatively predict the distribution of an inulin tracer perfused through the multi-organ human-body-on-chips. The automated culture system enables the imaging of cells in the organ chips and the repeated sampling of both the vascular and interstitial compartments without compromising fluidic coupling.

Vascularized human organ chips are microfluidic cell culture devices containing separate vascular and parenchymal compartments lined by living human organ-specific cells. Such systems recapitulate the multicellular architecture, tissue–tissue interfaces and relevant physical microenvironments of key functional units of living organs while providing vascular perfusion in vitro[1,2]. There is growing recognition that animal models do not effectively predict drug responses in humans[3–5] and a related increase in demand for in vitro human toxicity and efficacy testing. This has led to the pursuit of time-course analyses of human organ-chip models and fluidically linked, multi-organ, human-body-on-chip (HuBoC) systems that recapitulate organ-level functions to facilitate studies of the pharmacokinetics (PK) and pharmacodynamics (PD) of drugs in vitro[6–11].

An automated experimental system that can meet these goals needs to be highly multifunctional and must ideally enable fluid handling and sample collection, perfusion of fluid through multiple linked microfluidic organ-chip devices and tissue imaging all within a controlled temperature, humidity and CO_2 environment. Custom assemblies using syringe pumps[12], peristaltic pumps[13], micropumps[11,14,15] and gravity feed[10,16,17], including several commercial systems[18,19], can be used to perfuse and link microfluidic tissue and organ culture inside incubators; however, these systems do not provide the features necessary for complex HuBoC experimentation. In particular, these systems offer limited ability to sample the different biological compartments and lack the capacity to reconfigure the system so that the same system can be used for multiple

[1]Wyss Institute for Biologically Inspired Engineering at Harvard University, Boston, MA, USA. [2]CFD Research Corporation, Huntsville, AL, USA. [3]Disease Biophysics Group, Harvard John A. Paulson School of Engineering and Applied Sciences, Harvard University, Cambridge, MA, USA. [4]Department of Pathology, Massachusetts General Hospital, Boston, MA, USA. [5]Department of Bioengineering and iBB—Institute for Bioengineering and Biosciences, Instituto Superior Técnico, Universidade de Lisboa, Lisboa, Portugal. [6]Vascular Biology Program and Department of Surgery, Boston Children's Hospital and Harvard Medical School, Boston, MA, USA. [7]Department of Biology, University of Freiburg, Freiburg, Germany. [8]GlaxoSmithKline, Collegeville, PA, USA. [9]Harvard John A. Paulson School of Engineering and Applied Sciences, Harvard University, Cambridge, MA, USA. [10]Present address: Division of Micro and Nanosystems, KTH Royal Institute of Technology, Stockholm, Sweden. [11]Present address: Department of Biomedical Engineering and Sagol School of Neuroscience, Tel Aviv University, Tel Aviv, Israel. [12]Present address: Emulate, Inc., Boston, MA, USA. [13]These authors contributed equally: Richard Novak, Debarun Das, Anna Herland, Ben M. Maoz, Rachelle Prantil-Baun, Mahadevabharath R. Somayaji. *e-mail: don.ingber@wyss.harvard.edu

experimental designs. Other HuBoC systems have used manual or automated transfer of fluid flow between multiple microfluidic culture systems using gravity feed[10,16] or they have relied on perfusion through integrated microfluidic networks controlled by microvalve pumps[14,19,20]. But in these systems, the shared medium that contains the drugs was transferred directly from one parenchymal tissue type to another without passing through a vascular endothelium as normally occurs in vivo. This lack of endothelial barriers is a significant limitation in PK studies for which the endothelium can substantially contribute to drug absorption, distribution, metabolism, excretion and toxicity[21,22].

Here, we present a new approach to linking different organ chips for HuBoC studies, whereby liquid-handling robotics are used to overcome these limitations. Specifically, this approach relies on the automatic and regular robotic transfer of liquid samples between individual organ chips that are each continuously perfused. The liquid transfers act to replace direct fluidic plumbing (for example, through tubing or microfluidic channels), thereby avoiding various engineering complexities, such as priming, washing and a propensity to collect bubbles, while providing full reconfigurability and software-based control. Perfusion pumps are assigned to each of the organ chips to ensure that they experience continuous fluid flow independently of the action of the robotic fluid transfer system.

To include liquid-handling robotics and individual organ-chip perfusion in a format that fits within standard tissue-culture incubators, we developed a custom, modular system for culture and analysis, which we call an 'Interrogator' instrument (Fig. 1). In addition to automated culture, perfusion and fluidic coupling, we incorporated in situ imaging using a software-controlled mobile microscope. We also developed an Interrogator control environment that permits the on-demand reconfiguration of experimental protocols, routing of drug administration, media replenishment and analyte sampling, as well as organ-chip addition, removal and exchange. The system supports vascularized organ chips composed of polydimethlysiloxane (PDMS) or polycarbonate (PC) and contain two parallel, continuously perfusable microchannels separated by a porous membrane, which are seeded with living human organ-specific parenchymal cells and vascular endothelial cells on either side of the membrane to create a tissue–tissue interface[23,24]. The dimensions of the channels, the perfusion rate, the types of medium and the protein coatings can be varied to create organ-specific designs that optimize the surface area or, in the case of skin, that lack an upper surface of the upper channel to permit experimental access to the surface of the epidermis (Supplementary Fig. 1). The endothelium-lined vascular channel in each organ chip is perfused with a common 'blood substitute' universal medium (see Methods), while each parenchymal channel is perfused with organ-specific medium or exposed to an air–liquid interface (in the case of lung and skin) to more accurately emulate organ-level physiology and pathophysiology[1,25–33]. Some of the organ chips (that is, gut, liver, lung, blood–brain barrier (BBB) and skin) also contain hollow side chambers that run parallel to the central culture channels through which cyclic suction can be applied to mechanically stretch and relax the cultured tissue–tissue interface, thereby mimicking physiological tissue motions that occur in vivo (for example, breathing in the lung or peristalsis in the gut)[28,29,34,35]. Our studies demonstrate that the automated Interrogator instrument can be used to maintain multiple human vascularized organ chips for weeks in culture when fluidically linked. Using the Interrogator, it is also possible to emulate the physiological systemic transport of small molecules between organs through a common endothelium-lined vasculature and across the endothelium–parenchymal tissue interface of each organ, which is a major contributor to drug PK behaviour[2,22]. Importantly, the Interrogator was designed to enable versatile, modular operation and without a priori assumptions about organ-chip scaling, including allometric scaling of organ masses or metabolic rates. This instrument supports the execution of systematic organ-chip workflows for PK and PD analyses[7], including accounting for chip materials and geometries, drug properties and integration with

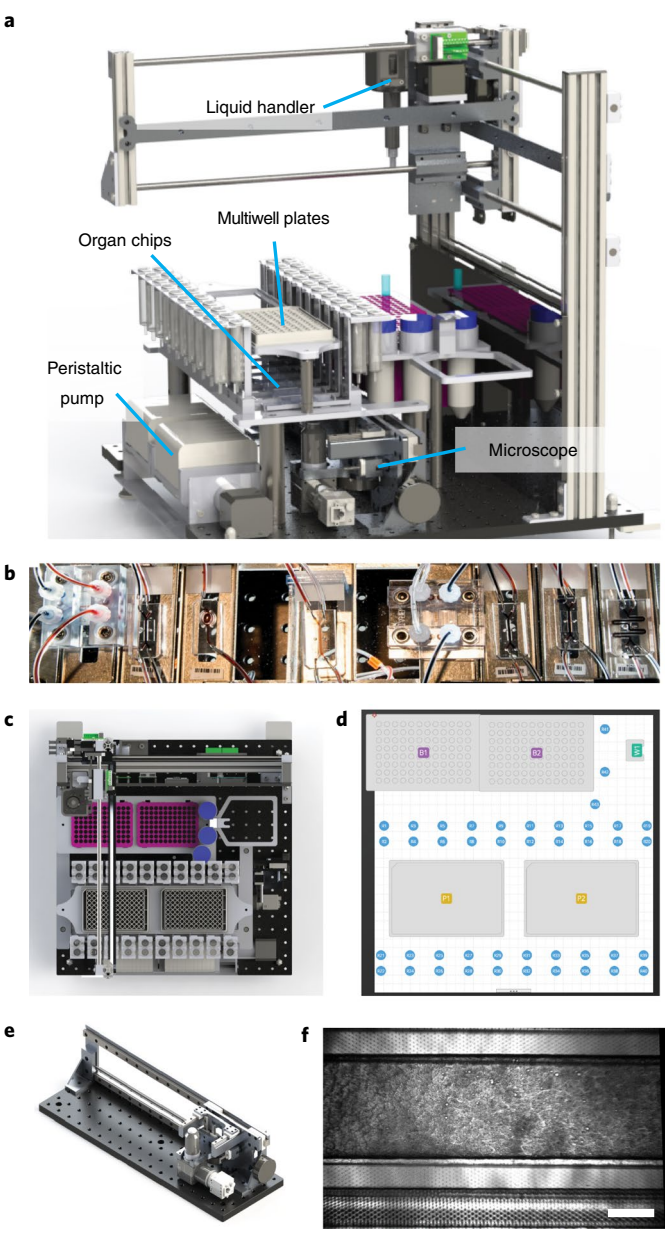

Fig. 1 | Overview of the Interrogator device. a, Rendering of the Interrogator CAD model. The system comprises a three-axis motion system, an automated liquid handler, a peristaltic pump and a custom microscope stage that allows for the continuous perfusion, linking and image analysis of organ-on-chip models. **b**, Organ chips are placed between inlet and outlet reservoirs in modular docks below the main fluid-handling deck. Left to right: brain, BBB, skin, lung, heart, kidney, liver and gut. **c**,**d**, Top view of the instrument deck layout in CAD (**c**) and within the graphical user interface (**d**). Component positions are determined from CAD and then used to build a virtual deck in the control software, which contains inlet/outlet reservoirs (blue), pipette tip boxes (purple), multiwell plates (yellow) and waste (green). **e**, Rendering of the microscope module, showing a compact optical path microscope mounted on a three-axis positioning stage that is integrated into the Interrogator for real-time imaging and inspection of organ chips. **f**, Micrograph of a gut chip channel showing villus-like structures. Scale bar, 500 μm. In **a**–**e**, the widest part of each object is 450 mm.

computational modelling. In a companion paper[36], we report the application of the Interrogator in a linked organ-chip model of first-pass metabolism to predict PK and PD parameters of two drugs, opening the path for HuBoC experimentation as part of the drug development process.

Results

The automated Interrogator was designed to be small (45 × 45 × 45 cm) so that it can fit within a standard tissue-culture incubator and provide continuous perfusion of up to ten organ chips for HuBoC studies using an integrated custom peristaltic pump module and fluidic coupling via their vascular channel reservoirs (Fig. 1). The Interrogator also enables automated sampling and dosing of chips by transferring samples of medium to and from wells of standard culture plates housed in the instrument and the inlets and outlets of the organ chips using a robotic fluid-handling device. In addition to experimental convenience, this automation reduces the frequency of incubator access, thereby stabilizing the temperature, oxygen, humidity, light and CO_2 levels experienced by cells. Indeed, continuous operation of the Interrogator was found to deviate the incubator temperature by <1 °C (Supplementary Fig. 2a,b). The instrument, which was fabricated in-house, permits the automated transfer of controlled fluid volumes (>50 µl) between arbitrary chips and reservoirs in a programmable manner for organ–organ linking and for experimental sampling (Supplementary Video 1). The system can emulate different drug delivery methods by delivering compounds to an arteriovenous reservoir that is linked to the vascular channels of all chips ('intravenous' delivery) or to the parenchymal channels of gut ('oral'), lung ('inhalation') or skin ('transdermal') chips. A server box lies outside the incubator to provide networked connection from a web application interface. Low-level electronics, including motorized axis controls and camera, are located within the incubator and can withstand the high humidity and CO_2 atmosphere. A standard USB cable and power cable are the only connections necessary for operation.

The Interrogator instrument is composed of multiple subsystems, including a three-axis motion system, an automatic liquid handler, a computer-controlled peristaltic pump and a microscopy imaging module (Fig. 1a). The configuration described here is designed to support up to ten different vascularized (two-channel) organ chips (Fig. 1b), while the deck layout is customizable and reconfigurable (Fig. 1c,d). Each organ-chip module features a completely independent peristaltic perfusion system consisting of two inlet reservoirs, all tubing connections and two outlet reservoirs. Perfusion rates between 1 and 10 µl min^{-1} were confirmed to be within 10% of the setpoint for at least 1 week (Supplementary Fig. 2c) and were selected based on perfusion rate ranges previously shown to induce organotypical physiology in organ chips[28,29]. Automated linking between organ chips is achieved by either direct and repeated pipetting of discrete volumes of medium from one chip outlet to the inlet of another chip or through an intermediate reservoir. This reconfigurability and modularity enables the user to change chip linkage order and experimental protocols without the need to physically move organ chips or change tubing connections, which can restrict the use of existing HuBoC systems. The instrument also contains a standalone microscope module (Fig. 1e,f) consisting of a three-axis miniaturized stage and a compact microscope with camera, which enables on-demand imaging of the organ chips without requiring cessation of fluidic coupling or removal from the incubator.

The custom software environment developed to control the Interrogator provides a graphical user interface for instrument deck setup, configuration of reservoirs and other consumables, experimental design and execution, and real-time experimental error-checking to pre-empt costly programming errors (Supplementary Fig. 3). Complex operations, such as multiwell sampling and serial dilutions, are handled using high-level functions to reduce programming time. The combination of an entirely graphical programming approach with high-level functions and integrated error-correction allows novice users to operate the Interrogator even for complex experimental protocols with time-varying perfusion rates (Supplementary Fig. 4). By using a web application stack, the system software allows for remote access to machines over a network through a central server computer (Supplementary Fig. 5). Multiple client browsers can communicate with a single Interrogator or a single client browser can communicate with multiple instruments; the hardware components of each instrument are connected to a Mac-Mini driver computer. The driver computer runs JavaScript code (see Methods) that translates the experiments and actions from the client into a set of machine motions to be run on each subcomponent sequentially and/or concurrently. Additionally, JavaScript was selected to simplify development of a user-friendly interface that is critical for adoption by a broad range of end users. The driver computer also provides constant updates to the client regarding machine component status and the overall machine state, including liquid levels, loaded consumables and current running experiment step. Networking the system enables remote experimental design, operation monitoring and deployment of software updates.

Using the microscope module of the Interrogator (Fig. 1e), still images and dynamic recording of organ actuation are equally possible, with the ability to visualize, for example, the villi-like morphology and the cyclic stretching of the gut chip by applying cyclic suction to the hollow side microchambers (Fig. 1f; Supplementary Fig. 1; Supplementary Video 2). The challenge of providing phase-contrast imaging, which is required for the noninvasive visualization of some tissues, was solved using a phase plate suspended between the organ-chip cartridges and a light-emitting diode (LED) array light source (Supplementary Fig. 6). Owing to the modular design, the alignment of the organ chips relative to the rectangular slits of the phase plate serve to structure light from an LED array to create a partial phase-contrast light source. The microscope controls allow regions of interest to be saved and returned to for time-lapse imaging, and to facilitate repeated inspection of the same regions of interest over time in the organ chips. We further designed an epi-fluorescence microscope module to expand the analytical capability of the system (Supplementary Fig. 6).

Interrogator characterization. An instrument calibration procedure was developed and validated by measuring the positional error of the system before and after calibration, which greatly improved positional accuracy (Fig. 2a,b). Before calibration, the instrument had positional errors of −4.07 to +1.70 mm across the three axes due to inherent variations in the parts, misalignment during assembly and deflection of the axes during operation (Fig. 2c). As expected, the positional errors for each axis were dependent on the position relative to the other axes (for example, the positional error of the z axis was dependent on the position of the x axis). Importantly, after calibration, the positional error for all three axes remained less than 0.5 mm (Fig. 2d), which facilitated robust interfacing with 96-well plates. The stability of each axis was tested using an automated routine of 1,000 cycles of motion through the full range of motion; success corresponded to maintaining positional stability to within 0.1 mm, which was accomplished throughout all cycles. The pipettor was also characterized for accuracy and precision of fluid handling using an automated serial dilution protocol and repeated pipetting of volumes. The standard dilution data were fit to a four-parameter logistic regression with a correlation coefficient of $R^2 = 0.9998$ (Fig. 2e). The pipetting error was less than 2% for volumes of 100 µl and above when using 1-ml pipette tips, and only 4% for a volume of 50 µl at the low end of the volume capability range for this pipette head and tip configuration (Fig. 2f).

The modularity of the system lends itself to numerous design configurations. For example, to develop model calibration parameters

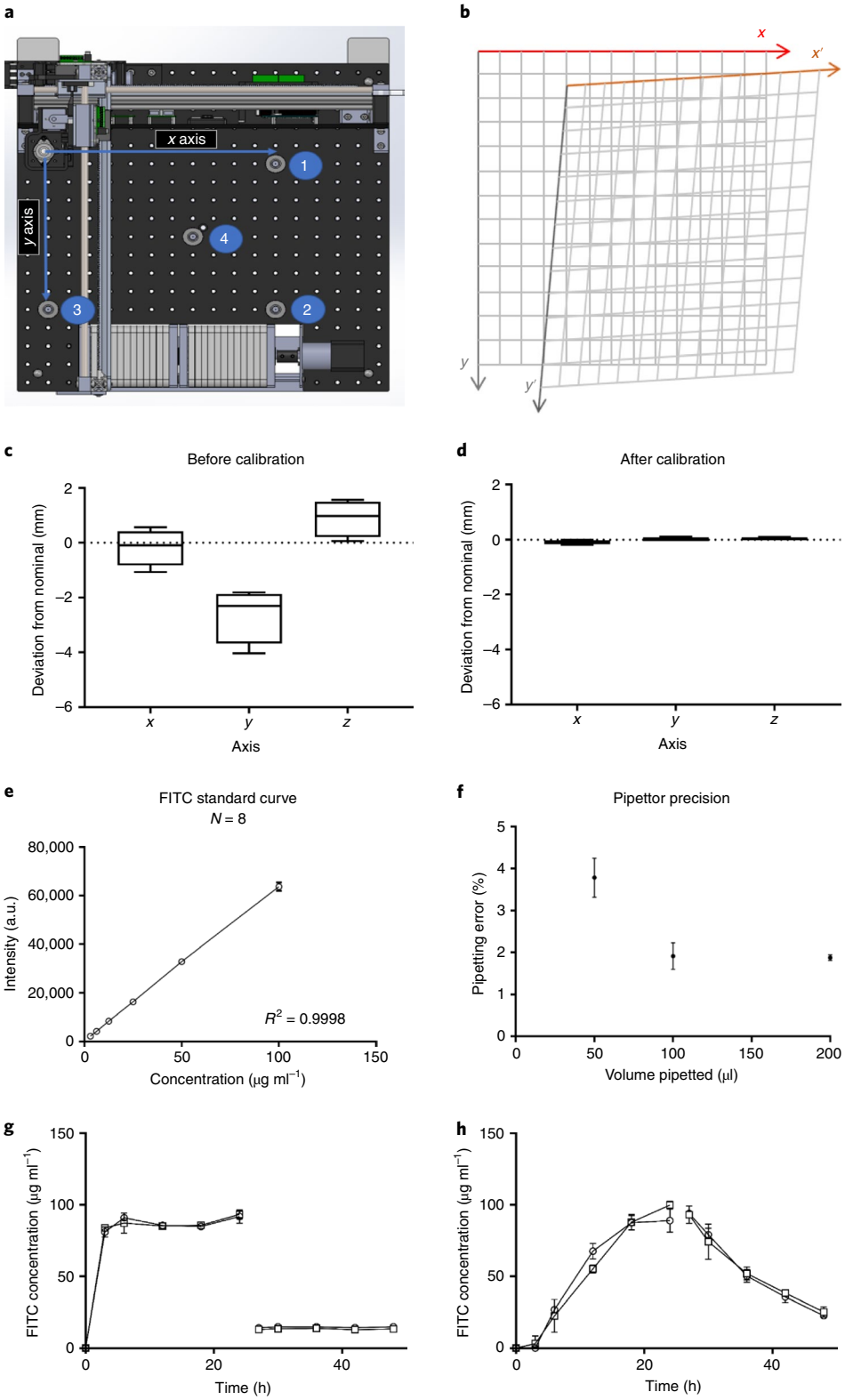

Fig. 2 | Schematic of stage calibration and system characterization. a, A matrix of *x*, *y* and *z* coordinates is corrected by touching the four calibration points (labelled 1–4) with a probe attached to the pipettor head. The area shown is 450 × 450 mm. **b**, The hardware coordinates are then mapped to the theoretical coordinate matrix to generate a calibration matrix that is automatically used to adjust the fluid-handler stage motion. **c**,**d**, Initial positional errors (**c**) can be reduced below 0.5 mm (**d**). Boxplots indicate the means, interquartile ranges and minima/maxima. **e**, The accuracy and precision of the liquid handler used in organ-chip linking studies was measured using a standard dilution routine of fluorescent dye ($N = 8$). **f**, The accuracy of the pipettor was calculated as follows: error = s.d./mean. Error bars represent the s.e.m. of error and correspond to the precision ($N = 60$). Automated generation of absorption/adsorption calibration data using empty organ chips and inulin-FITC tracer dye during infusion and elution phases of $N = 3$ independent replicates. **g**,**h**, The inlet reservoirs (**g**) show the addition of fluorescent tracer for the first 24 h, while the outlet reservoirs (**h**) exhibit dye dilution due to perfusion through the organ-chip device. Mean and standard error of the mean values are shown in all plots.

for an inulin-fluorescein isothiocyanate (FITC) tracer dye that is commonly used to characterize tissue-permeability barriers in vivo[37–39], as well as in organ chips[24,29,40], the Interrogator was used to determine tracer distribution. The absorption and adsorption of the tracer by the PDMS chips and associated materials under conditions in which perfusion was carried out using empty organ chips without cells were also evaluated. The Interrogator automatically executed the tracer dosing and elution study by pipetting a solution containing the fluorescent tracer into the apical and basal inlets of chips fabricated with membranes lacking pores, perfusing medium through the apical and basal channels of the organ chips using the integrated peristaltic pump and performing robotic sampling of their outlets over 24 h. This was followed by a 24-h washout phase during which the pipettor introduced fresh medium into the inlets without tracer dye. Inlet fluorescence rapidly reached steady state during the infusion phase (Fig. 2g), while a gradual increase in fluorescence intensity was seen in the outflow samples (Fig. 2h). In addition, desorption of fluorescent tracer was observed during the washout phase (Fig. 2h), and these measurements were then used in the quantitative analysis of a HuBoC system containing eight different human organ chips fluidically linked using the Interrogator instrument. In addition to focused instrument characterization, these studies consisted of thousands of individual automated mechanical actions over the span of several weeks, further supporting the robustness of the robotic system in real-world scenarios.

Failure modes. Throughout testing and initial experimentation, initial failure modes included connectivity issues, perfusion instability due to bubbles and debris, evaporative fluid loss and organ-chip contamination. Connectivity, particularly during periods of unstable network performance, could be temporarily addressed through hosting the client and server locally. Perfusion instability was generally observed at the onset of a study due to the introduction of bubbles, which was countered with plasma treatment of all tubing and connectors before the start of the study. Perfusion instability at several weeks of perfusion was more likely to be caused by debris, such as Caco-2 cell sloughing, collecting in the perfusion channels and tubing. Both sources of perfusion instability were resolved by incorporating higher velocity flushes (5 µl min^{-1}) every 1–12 h; 4-h intervals were found to be optimal for eliminating perfusion imbalances with minimal additional perfused volume. Evaporative loss and organ-chip contamination were reduced by the addition of scored plate sealing films on all reservoirs. Over many studies, contamination was dramatically reduced by implementing a 24-h quarantine procedure for chips before the start of the study, whereby chips were perfused but not linked. This enabled the isolation of contaminated chips and prevented them entering the linked fluidic system.

Leveraging the Interrogator to create an automated HuBoC system. Given its capabilities, the Interrogator instrument should enable a range of studies from the automated culture of single organ chips or the coupling of chips for first-pass metabolism to more complex whole HuBoC analysis. To create a HuBoC system, we used the Interrogator to fluidically link, perfuse and culture eight different human organ chips representing the intestine, liver, kidney, lung, heart, skin, BBB and brain. These chips were lined by human parenchymal cells from each of these organs in one channel and by vascular endothelium in the parallel channel (Fig. 3). The vascular endothelium consisted of human umbilical vein endothelial cells (HUVECs) except where indicated. The methods for creating each of these chips have either been published[13,31,34,35,41] or are described in the Methods; note that to increase the absorptive surface area of the gut chip, the channels were lengthened five times relative to previous publications by creating a serpentine pattern on the chip (Fig. 3a). Where possible, an attempt was made to minimize differences in chip design

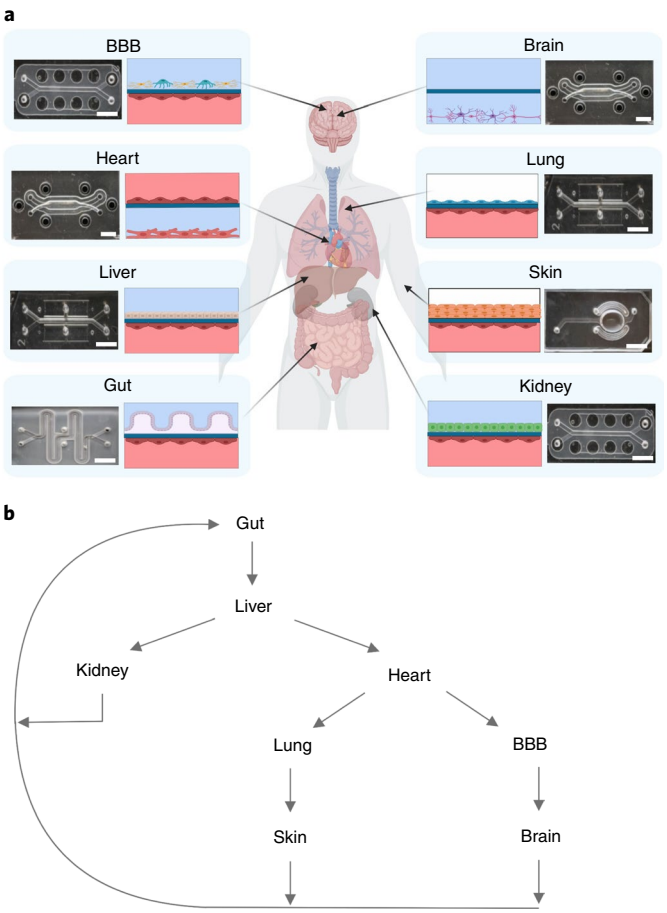

Fig. 3 | Linking scheme of eight organ HuBoCs. a, Human organs for the HuBoC system, each with a representative organ-chip photograph and sectional schematic. BBB: the lower channel contains brain microvascular endothelial cells, while the upper channel contains brain pericytes and cortical astrocytes. Brain: the chip contains differentiated human primary neural stem cells forming networks of neurons and astrocytes. Lung: the lower channel contains HUVECs, while the upper channel contains lung epithelial cells. Skin: the lower channel contains dermal microvascular endothelial cells, while the upper channel contains keratinocytes and dermal fibroblasts. Kidney: the lower channel contains kidney-derived endothelial cells, while the upper channel contains proximal tubule epithelial cells. Gut: the lower channel contains HUVECs, while the upper channel contains villi-like structures of gut epithelial cells. Liver: the lower channel contains liver sinusoidal endothelial cells, while the upper channel contains hepatocytes. Heart: the lower channel contains HUVECs, while the upper channel contains stem cell-derived cardiomyocytes. Scale bar, 5 mm. **b**, A total of eight vital organs—gut, liver, heart, kidney, lung, heart, brain, BBB and skin—were joined through vascular endothelial channels to create the body on chips. The system enables multiple sampling points and a variety of linking possibilities.

to facilitate chip fabrication and to streamline parameter determination and modelling, and the modularity of the Interrogator supported biologically driven organ-chip design modifications. Each of the organ chips was cultured until it reached a mature state, as determined by measuring organ-specific functions (that is, intestinal villi formation and barrier function; liver albumin production; kidney albumin reabsorption; heart contractility; lung barrier function; skin cell differentiation and barrier function; BBB permeability function (Supplementary Fig. 7)), and the time required differed depending on the organ type (Supplementary Fig. 8).

These organ chips were fluidically linked using the robotic fluid-handling module to mimic oral dosing of a compound through the lumen of the intestine chip and subsequent distribution to the body. The apical channels were perfused at the same rate as the basal vascular channels, and fluidic linking was carried out every 12 h by transferring and thoroughly mixing small volumes (62.5–250 µl) of blood substitute culture medium from the outflows of the organ-chip vascular channels to the inlets of the other linked organ chips in the order described in Fig. 3b. This intermittently linked fluidic network was maintained at a 1 µl min^{-1} flow rate; periodic 5 µl min^{-1} flush cycles (every 4 h) were also automatically applied using the integrated peristaltic pump and control software to dislodge any debris or bubbles that could impede perfusion during the 3 weeks of culture. This flow rate resulted in fluid transit from the inlet reservoir to the end of the organ-chip culture region in ~120 min; note that specific drug properties may affect this rate, and all compounds were individually tested using empty chips. Because the vascular channels within the organ chips were lined by a continuous endothelium, it was possible to perfuse multiple different linked organ chips with a single endothelial medium—the blood substitute—to mimic in vivo blood perfusion of multiple organ systems. We evaluated endothelial compatibility with specific media, including complete commercial endothelial media, without success. Decreasing the serum level in a commercial medium (EGM2) resulted in increased endothelial monolayer stability. Owing to the automated fluid-handling capabilities, the incubator environment was not subject to temperature and CO_2 fluctuations that could perturb tissue function beyond brief plate and pipette tip exchanges every 24 h.

The automated Interrogator instrument effectively maintained perfusion, viability, morphology and organ-specific functions of all eight organ chips throughout the entire 3 weeks of fluidically linked perfusion culture in two separate studies (Fig. 4). The responses of the HuBoC organ chips were analysed once a week with multiple organ-specific structural and functional assessments, including immunostaining for vascular endothelial (VE)-cadherin to measure endothelial integrity on all chips (except the brain chip, which did not have an endothelium as it was linked to the BBB chip); VE-cadherin was chosen because it is detected in all organ-specific endothelia, including liver sinusoidal endothelium[42]. ZO-1 was used to assess epithelial integrity in the gut, lung and kidney chips, and apparent permeability (P_{app}) values for inulin-FITC, dextran (3 kDa) or Cascade Blue (596 Da) were also used to estimate barrier function in the gut, lung and skin chips, respectively. MRP2 staining of hepatocytes and albumin production levels were used to assess the liver chip, whereas kidney chip function was measured by quantifying albumin reabsorption. Analyses of α-actinin staining and lactate dehydrogenase (LDH) release were used to analyse cardiomyocytes in the heart chip, whereas epidermal cells were stained with loricrin and keratin 14 in the skin chip. Glial fibrillary acidic protein (GFAP) staining and LDH release were used to measure the function and viability of astrocytes and pericytes in the BBB chip, and brain chip function was assessed by staining for astrocytes (using GFAP) and neurons (using class III β-tubulin) and by quantifying the glutamine/glutamate ratio via mass spectrometry. Immunofluorescence staining of these various cell markers confirmed the maintenance of tissue-specific morphology and relevant distributions of molecular markers in all organ chips (Fig. 4, upper) and confirmed low cell-death rates.

To verify the control of medium perfusion throughout the entire HuBoC in vitro model and to quantify the distribution of soluble small molecules, we infused inulin-FITC tracer dye 'intravenously' into the vascular channel of the gut chip once every week to mimic the distribution of a small molecule or drug immediately after it has been absorbed through the intestine lumen into the vasculature. The tracer dye concentrations were highly reproducible in all organ chips when measured every day over the 3-week period of culture (Fig. 5). This result confirms the stability of the fluidically linked HuBoC system and all levels of Interrogator operation, from perfusion rates to pipettor distribution and sampling accuracy to maintenance of organ-chip barrier function over 3 weeks of linking.

To further understand whether the distribution of the inulin-FITC tracer within the linked organ chips of the HuBoC system was quantitatively relevant (that is, in addition to being stable and reproducible), we developed a physiologically based multicompartment reduced-order (MCRO) computational model of the linked organ chips derived from spatiotemporal transport equations that account for accumulation, convection, diffusion and reaction processes. First, detailed three-dimensional (3D) simulations of the organ chips were created, incorporating convection and diffusion mass transport and physicochemical material properties of absorption and adsorption for each of the specific organ-chip and fluidic-linkage geometries (Supplementary Fig. 9). As the same chip designs were used for the gut, kidney, liver and BBB chips, we used the standard organ-chip model to simulate these chips; specialized models were created for the lung, skin, heart and brain chips (Supplementary Figs. 10–12).

The model was calibrated for inulin-FITC absorption and adsorption kinetics using the data shown in Fig. 2g,h. To accelerate the simulation time, we converted the computationally intensive 3D computational organ models into reduced-order systems of ordinary differential equations. Using this approach, we developed fast-running MCRO models for all planar organ-chip designs except the heart chip, for which a 3D model was used to capture the motion of the cantilevered muscular (cardiomyocyte) thin films that are included in the parenchymal channel of this chip (Supplementary Fig. 12; Supplementary Video 4). These reduced-order models were treated as convective-diffusive plug flow reactors rather than the commonly used well-stirred reactors, which more accurately mimics in vivo organ perfusion and provides meaningful residence time information. This in vitro MCRO model solves convection-diffusion-partition-reaction equations for species in the perfusing media, in cellular barriers, in membranes and in the PDMS package material. Importantly, this MCRO model recapitulated the experimental concentrations of inulin-FITC over time within all eight organ chips with good agreement (Fig. 5; Supplementary Video 5), which confirms that the Interrogator instrument enabled robust quantitative experimentation in multiple linked organ chips within this HuBoC system. An analysis of organ-specific assays at the conclusion of the tracer study once again confirmed that the functions of all eight organ chips were maintained over 3 weeks, even when subjected to this automated experimental protocol (Fig. 3).

Discussion

The ability of animal models to quantitatively predict drug toxicity and efficacy in humans is limited, which has prompted significant efforts focusing on developing human in vitro models for PK and PD testing[1,6,43,44]. Vascularized organ chips can recapitulate human organ-level physiology, as their two-compartment, semipermeable membrane structure mimics in vivo communication and mass transport across physiologically relevant tissue–tissue interfaces with the endothelium-lined vasculature[1,2]. In addition to mimicking healthy organ physiology, organ chips have recapitulated pathophysiological conditions, including chronic obstructive pulmonary disease, tobacco smoke exposure, asthma and viral infections in the small airway[45,46], bacterial infections[34,47] and radiation exposure[48] in the gut, and drug toxicities in multiple organ chips[31,40,49]. While these approaches highlight the value of single-organ chips, PK and PD analyses require multi-organ or whole-body systems linked by vascular perfusion.

Here, we described an automated Interrogator instrument that can perfuse and fluidically link up to ten different human organ chips and maintain their viability and function for at least 3 weeks in

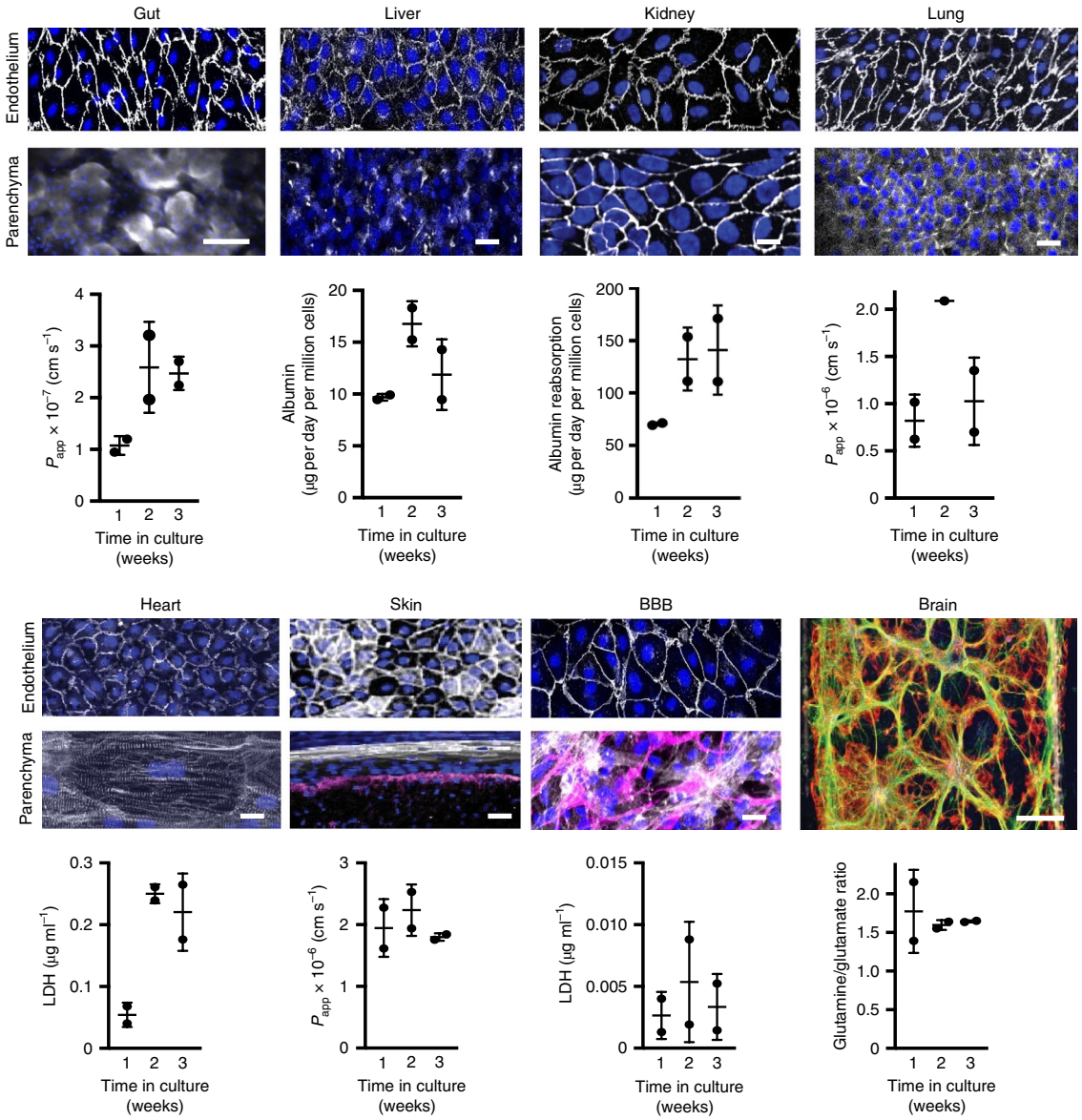

Fig. 4 | Automated HuBoC linkage demonstrates maintenance of organ viability and function for 3 weeks. Immunofluorescence imaging of the HuBoC organs (upper rows) and organ-specific assessment (lower rows) throughout 3 weeks of linkage. For each organ chip, the following stains were used (for all organs, VE-cadherin was used to stain for endothelium unless otherwise stated) and parameters analysed. Gut: ZO-1 for parenchyma and permeability values for inulin-FITC. Liver: MRP2 for parenchyma and albumin production. Kidney: ZO-1 for parenchyma and albumin reabsorption. Lung: ZO-1 for parenchyma and dextran (3 kDa) for permeability. Heart: α-actinin for parenchyma and LDH secretion. Skin: white loricrin and purple keratin 14 for parenchyma and Cascade Blue (596 Da) for permeability. BBB: white pericytes, purple astrocytes (GFAP) for parenchyma, and LDH secretion. Brain: green astrocytes (GFAP) and red neurons (class III β-tubulin) for parenchyma, and glutamine/glutamate ratio. Scale bars, 100 μm. Data were recorded at the given time points from two independent experiments, and micrographs were acquired from unlinked control chips following 3 weeks of culture. The immunohistochemistry values are representative of multiple organ chips and chip regions from approximately six to eight images taken per condition. Data are from two independent studies, with mean and s.d. values shown in all plots.

culture using a common blood substitute medium. Although robotic fluid handlers have been previously used for microfluidic tissue culture, the Interrogator represents a system that is capable of complex, programmable experiments using perfused single or linked organ chips. The robotic Interrogator instrument supported organ-chip culture through integrated perfusion, automated replenishment of media, precision fluid transfer between linked organ chips, and sampling of organ-chip inlets and outlets for analysis of inulin-FITC distribution. We also demonstrated that the Interrogator can be leveraged to create a viable HuBoC system that maintains multi-organ function for at least 3 weeks in vitro. Although only a branched serial linkage scheme with eight organ chips was used here, robotics-based organ linking can be readily reconfigured to include varying numbers of organs and an arteriovenous reservoir, as shown in a companion paper[36]. The modular design of both the Interrogator hardware and control software enables the rapid addition or removal of organ chips without disrupting the experiment, including, importantly, the perfusion of media. The dosing of drugs can be modified to any mode of delivery, whereby oral dosing to the gut, intravenous dosing to the interconnected vascular medium, topical skin dosing and aerosol dosing to the lung are all feasible to integrate. The modularity of our HuBoC approach also facilitates

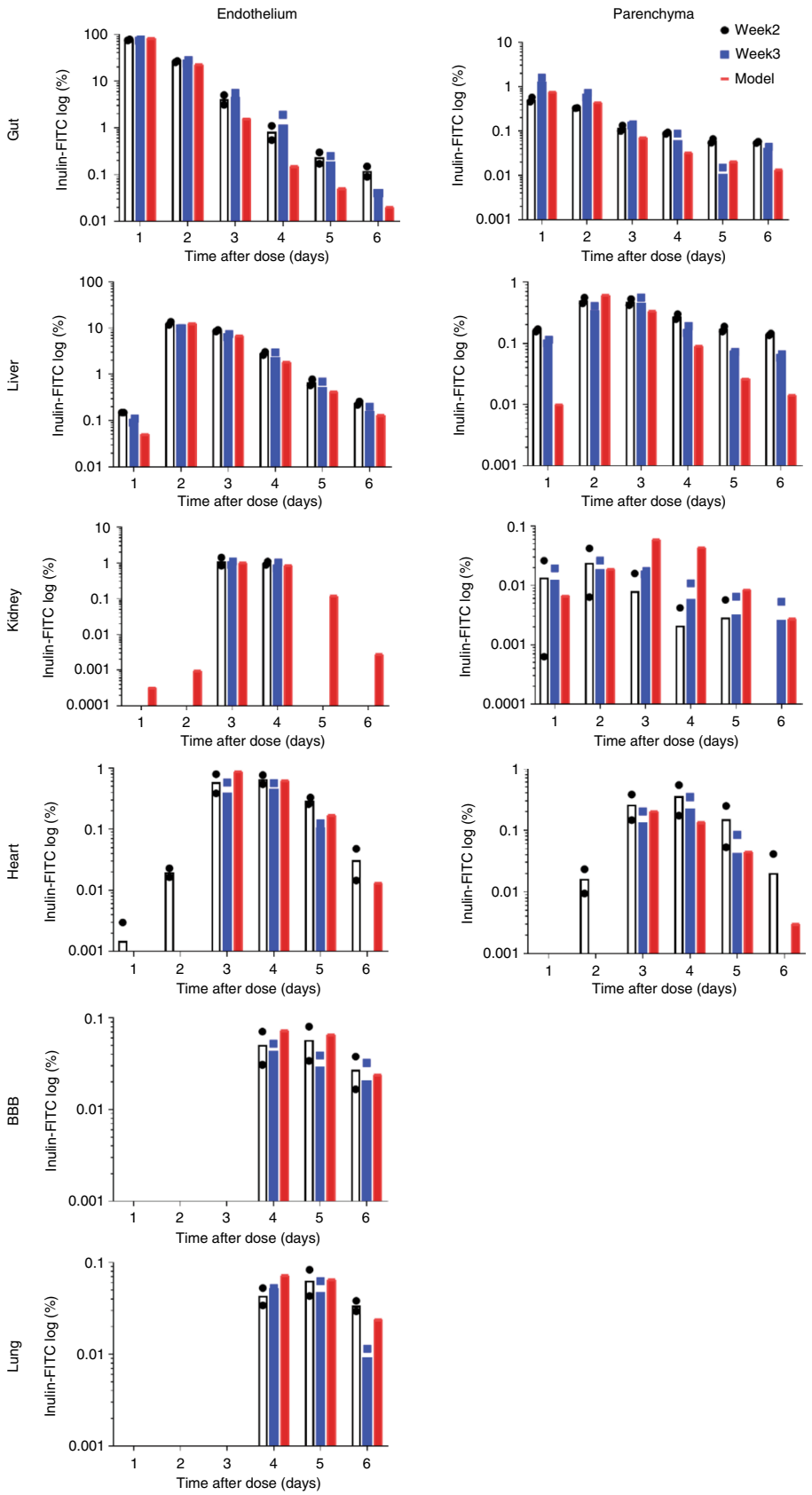

Fig. 5 | Long-term analysis of inulin-FITC PK in an eight organ system linked via vasculature and supported by computational PBPK modelling. The tracer dye inulin-FITC (2–5 kDa) was given as a bolus dose once a week on the parenchymal side of the gut chip and linked as shown in Fig. 3. Experimental values (white bars, days after dose of the second week; blue bars, days after dose of the third week) for inulin-FITC concentration throughout the linked organ chips match the PK model predictions (red bars) over 21 days in both the endothelial and parenchymal channels. Data from two independent studies shown. Readouts below 0.005% are at the limit of detection. Mean and s.e.m. shown in all plots.

time-delayed linking of organs (for example, to mimic the temporary loss of organ function or perfusion) and isolation of organ subsystems, which would be difficult or impossible in animal models. Critically, the Interrogator design is agnostic to the scaling of organ chips and therefore provides a versatile system for exploring scaling rules and the impact that the underlying assumptions may have on PK analysis.

The Interrogator facilitated the experimental design and model calibration for complex studies of linked organ chips within a HuBoC system. Error checking integrated into the control software prevented mistakes in the fluid-handling programming by continually simulating the input values to assess physical feasibility, accounting for organ-chip perfusion over time, and volume changes due to sampling, linking and media replenishment. Furthermore, the software alerted users if inadequate pipette tips or media volumes were present. The precision of the data obtained from Interrogator-automated collection of time-resolved samples during empty organ-chip perfusion and complex linking of arbitrary organ chips facilitated the calibration of MCRO computational models of the experimental design. This in turn enabled the analysis of experimental data, which would otherwise be difficult to validate, and showed in vitro and in silico agreement. This approach can be further exploited to optimize experimental conditions in silico by enabling the simulation of tracer distribution through the linked organ chips to assess optimal sampling time points and study duration. The capabilities enabled by the Interrogator demonstrate how close the interplay between computational and experimental efforts may accelerate PK and PD experimental design and data analyses in HuBoC systems[7].

Physiologically based PK (PBPK) models have relied on conventional in vitro cell culture devices, such as Transwells, to determine specific input parameters, such as drug solubility, barrier function, drug partition coefficients, intrinsic clearance rate in the liver and renal clearance rate in the kidney[50,51]. However, these static, quasi-equilibrium, in vitro systems cannot replicate key dynamic physiological organ characteristics; for example, microorganization of tissues within organs, perfusion of blood and other bodily fluids that affect drug metabolism and transport, time-dependent dosing of drugs and metabolites that cross back and forth across the endothelial–tissue interface, organ–organ interactions, and chemical, biological and physical microenvironments specific to the respective tissues. Mathematical in vitro-to-in vivo extrapolation models have been developed to address some of these limitations, but these often fall short due to nonphysiological scaling factors and organ structure assumptions (for example, the liver is viewed as a well-stirred reactor)[52,53].

Microfluidic organ-chip devices with perfused endothelial and parenchymal channels and multi-organ microphysiological systems have the potential to overcome these limitations[6,7,9,54]. For example, unlike most PK models, here, we leveraged the biomimetic design of organ chips to conduct full 3D simulations of mass transport without the pitfalls of well-stirred reactor assumptions. Incorporating the fundamental equations of previous PBPK models[52,55] and adapting them to describe a more physiologically accurate in vitro experimental system resulted in the MCRO model described here. Importantly, the equations we derived are also equally applicable to analyse human organ mass transport in vivo to better model human physiology[54]. This model and the simplified reduced-order differential equation models were used to confirm the quantitative accuracy of the Interrogator-enabled HuBoC system using an inert inulin-FITC tracer dye in the present study, which focused on the validation of the Interrogator instrument and did not attempt to incorporate allometric or other forms of scaling. However, in a companion paper[36], we show that this model can be extended to create a MCRO model that incorporates drug transport and metabolism with subsequent in vitro–in vivo translation. Both efforts are examples of applying the previously published theoretical workflow for organ-chip experimentation, which outlines the steps required for conducting and analysing organ-chip studies using any organ-chip material or tissue type together with any compound of interest[7]. The Interrogator provides a way to accelerate the workflow from single-chip parameter determination (for example, for analysing PDMS sorption in specific geometries) to fully linked-chip-system PK determination consisting of arbitrary materials and organ types.

While others have demonstrated fluidic linking of multiple microfluidic devices, they were each linked by a single type of organ parenchymal cell (for example, liver, lung or kidney epithelium)[10,56]; thus, their lack of a separate vascular compartment with associated flux between the parenchymal and vascular spaces limits their use in PBPK models and extrapolation to humans. Furthermore, the direct contact of parenchymal tissues with a shared medium not only poses a significant technical challenge for developing a universal blood substitute that all cell types can tolerate, but it may hinder normal tissue function by forcing parenchymal cells of different organs to directly interact, which does not occur in vivo. We leveraged the barriers to flux of oxygen, molecules and other compounds in organ chips resulting from the organization of tissues, perfusion of media and the materials of the chips themselves to more closely model in vivo physiology[57]. The Interrogator enables concurrent experimentation with linked devices consisting of different materials and properties, as demonstrated here with PDMS and PC chips. Several microphysiological systems have incorporated tissue culture well inserts with semipermeable membranes lined by both parenchymal cells and endothelial cells to develop a more physiological shared medium for linked organs[11,19,20]. Others have demonstrated the 3D culture of endothelial cells with a parenchymal tissue in single-organ configurations[58], which facilitates a shared medium but presents additional variability in the vasculature area for PBPK calculations. Despite these efforts to incorporate a shared vasculature, the lack of perfused parenchymal compartments in these systems still hinders PK and PD modelling as it does not incorporate the in vivo-like convection across parenchymal tissues that is present in nearly all organs (for example, urine flow, bile flow and cerebrospinal fluid flow).

The Interrogator-enabled HuBoC system approach presented here addresses all of these problems simultaneously in the following ways: (1) organ chips have parenchymal channels perfused with a relevant interstitial fluid that are interfaced across a semipermeable membrane and with an endothelium-lined channel that is perfused by a shared universal blood substitute medium; (2) fluidic linking can be arbitrarily programmed, before or during an experiment, and can entail arbitrary sampling schedules and linking of parenchymal media (for example, BBB parenchyma to the neuronal compartment in the brain chip, as demonstrated recently[13]); and (3) the HuBoC linkage is amenable to first-principles-based in silico modelling using equations that can apply to human physiology in vivo as well as to organ chips in vitro. The ability to use a universal medium across organ chips dramatically increases experimental flexibility by leveraging the Interrogator for HuBoC linking. Moreover, the potential to arbitrarily reconfigure the linkage scheme without the need to individually assess the viability of each new organ-chip linkage is another advantage of the Interrogator. The modular capability can be further extended to include primary or induced pluripotent stem cell organ-chip models as we have previously demonstrated[48,59]. In a companion paper[36], we report the utility of this versatile Interrogator-enabled HuBoC approach coupled with MCRO modelling for evaluating drug PK and PD in a first-pass organ-chip system. Indeed, we were able to recapitulate clinical drug profiles and PK parameters for two drugs (nicotine and cisplatin) previously observed in humans. In contrast to this work, we observed that the Interrogator may be most powerful when applied to smaller linked systems due to the technical challenges associated

with the concurrent culture of large numbers of diverse organ-chip types. We leveraged the Interrogator to obtain larger datasets for two drugs and demonstrated the application of the Interrogator for PK estimation using computational models. Applying this automated system to achieve larger replicates of linkages may be helpful for the investigation of new compounds by providing greater statistical power to probe physiological functions of interest.

There is a growing need to automate many biological in vitro experiments for improved accuracy, increased throughput and reduced risk to researchers when working with pathogens or other laboratory hazards. The compact Interrogator is a versatile tool that can be used for time-resolved studies in biocontainment scenarios whereby human experimenters could be placed at risk, such as when studying the pathogenesis of human viral and bacterial infections or developing chemical weapon countermeasures. The robotic system offers a modular, fully programmable design for organ-chip experimentation, whether using individual multichannel or single-channel chips, or a more complex HuBoC system. This in vitro human experimentation system, coupled with physiologically based MCRO modelling, may accelerate the development of more effective therapeutics and medical countermeasures, reduce the potential for drug toxicity and optimize the design of drug dosing regimens.

Methods

The Interrogator is mounted on a 450 × 450 mm aluminium optical board base (Thorlabs) to allow for insertion into most standard tissue-culture incubators. The system consists of a pipettor (Z-Series Pipette Pump 0949, Tricontinent) and control board (M-Series Controller PCBA 0955, Tricontinent) mounted on a custom three-axis gantry. The motion system consists of *x*–*y* stepper motors (Adafruit 324) paired with a 14–1/2° pressure angle 32-pitch rack and 16-tooth pinion system. The *z* axis comprises a stepper motor and screw drive (RoboDigg 11HY0401-200T52). Limit switches are used on the proximal end of all three axes, with a 1-mm homing offset. The gantry is controlled via g-code commands sent to a GRBL Arduino shield (settings described in Supplementary Fig. 13). Perfusion is achieved using two stacked 12-channel peristaltic pump heads (DG-12-B/D, Longer Pump) controlled by a geared stepper motor and custom controlled via an Arduino. Individual organ chips are mounted in stainless steel cartridges that each hold two inlet and two outlet reservoirs. Cartridges are snapped into a spring-loaded carrier tray and tubing is connected to the peristaltic pump. Two standard culture well plates, two pipette tip boxes and a waste collection bag are mounted in the rest of the platform deck.

Validation of the Interrogator. The gantry was optimized and validated by speed testing until failure to establish maximum speed set points, motion stability testing to within 0.1 mm over 1,000 motion cycles, and positioning accuracy and precision across the platform by puncturing 96-well plates using a pipette tip. The peristaltic pump was validated for perfusion stability and accuracy using a Sensirion SLI-0430 flow meter over 72 h. Pipettor accuracy was assessed using automated dilution of fluorescein dye, and precision was measured by 48 repeated transfers of fluorescein dye at 100 and 200 µl volumes.

Microscope module. The microscope module was designed using SolidWorks (Dassault Systèmes; see Supplementary Information for the computer-assisted design (CAD) files) and shown in Fig. 1e. The three-axis positioning stages were machined from corrosion-resistant aluminium 6061. Acme-threaded rods were coupled to pancake stepper motors (44M100D, Portescap) for compact actuation capability, and dual rails with ball-bearing carriages were used for smooth translation movement of the separate axis assemblies. The motors were driven via a GRBL shield mounted on an Arduino Uno controlled through Python. The mechanical components of the microscope module were bolted to the optical breadboard base of the fluid-handling robot.

The optical subassembly of the microscope consists of 1-inch diameter optical tubes (Thorlabs SM1 series) connected to a mirror cube and Nikon objective adapter ring. In this study, a ×10 Nikon phase-contrast objective was used. Images were acquired via a Python script from a camera (Basler, cA2500–14um). The image was focused using a 50-mm focal length achromatic doublet lens (Thorlabs, AC254–050) via a 100-mm focal length lens to reduce the optical path distance. To provide appropriate illumination for observing delicate cell features across the imaging area without a condenser, a phase plate was designed to be interchanged with the multiwell plate holders. The phase plate (Supplementary Fig. 6) consisted of a black acrylic sheet, laser cut with slits that correspond to the objective phase ring diameter. Illumination for the microscope assembly was provided by a strip of white LEDs mounted to the top inner surface of the incubator.

Software architecture. A JavaScript web interface communicates with the hardware of the system via a server, enabling remote control and troubleshooting access. The web interface facilitates experimental protocol setup using a completely graphical user interface. Users can set up reservoir and culture well plate locations, program fluid transfer time points and control the perfusion system in an integrated display. In addition, the user interface contains real-time volume calculation during the experimental design step that incorporates volume changes due to perfusion and fluid transfers, offering a layer of error correction to accelerate experimental program validation.

The web application uses a variation of the MEAN stack application. The MEAN stack is composed of NodeJS and ExpressJS as the server, MongoDB as the database and AngularJS as the front-end model-view-controller framework (Supplementary Fig. 5). The benefit of the MEAN stack is that it is written completely in Javascript, thereby requiring less cross-language data parsing and developer knowledge overhead. The control software uses a specific construction of the MEAN stack, called Angular Fullstack with the addition of SocketIO, for real-time socket communication between the client, the server and the machine. Numerous tutorials on the MEAN stack and SocketIO can be found online.

Liquid-handler characterization. Precision of the liquid-handling system was characterized by programming the three-axis robotic pipettor to create a serial 2× dilution using inulin-FITC dye and then measuring the fluorescence of the solutions using a BioTek Synergy Neo plate reader with 485-nm excitation. Eight replicates of the dilution series were pipetted to allow statistical analysis. Thorough mixing was performed before and after each transfer.

Reproducibility was measured by pipetting aliquots of 100 µg ml^{-1} inulin-FITC solution from a supply reservoir to a 96-well plate and then measuring the fluorescence using a plate reader as described above. Aliquots of 50, 100 and 200 µl were pipetted in two batches of approximately 30 samples per condition in two separate experiments. The mean and standard deviation of each volume within an experiment were used to calculate accuracy, and the mean and standard deviation between experiments were used to calculate reproducibility.

Microfluidic device fabrication. The gut, liver, lung, kidney, skin and BBB chips were fabricated as previously described[23,24,60]. Briefly, moulds for the microfluidic devices were fabricated out of Prototherm 12120 using stereolithography (Protolabs). The top and bottom components of the devices were cast from PDMS at a 10:1 w/w base to curing agent ratio and bonded to a porous PDMS membrane using oxygen plasma (Atto, 30 mbar O_2, 50 W, 2 min; Diener Electronic). The membranes provide a semipermeable barrier between the epithelium and microvascular endothelium layers and were fabricated by casting against a deep reactive-ion etching (DRIE)-patterned silicon wafer (50 × 50 mm) consisting of 50-µm high, 7-µm diameter posts spaced 40-µm apart. Chips with PDMS membranes enable application of cyclic strain via programmable sinusoidal vacuum pressure applied to the vacuum ports parallel to the fluidic channels. Chips fabricated with polyester terephthalate track-etched membranes were assembled using (3-glycidyloxypropyl)trimethoxysilane (Sigma, 440167) and (3-aminopropyl)triethoxysilane (Sigma, 440140) as previously described[60]. Detailed chip dimensions are described in Supplementary Table 1 and chip cross sections are show in Supplementary Fig. 1.

The heart chip was composed of two PC parts and a porous membrane. The two PC parts were designed using SolidWorks software (SolidWorks) and produced by micromachining. The PC parts were then sonicated twice for 15 min in soapy water and once in water to remove residual oils from the machining process. Thereafter, the PC parts were dried with condensed air and incubated overnight at 65 °C for drying. To polish the surfaces, the PC parts were briefly exposed to dichloromethane (Sigma-Aldrich) vapours and dried in a dust-free environment at room temperature for 24 h. The PC porous membrane was cut with a ultraviolet laser (Protolaser U3, LPFK Laser and Electronics). The chip was placed in a vacuum chamber containing 4 ml of dichloromethane for 30 min to allow bonding of the parts. The PC porous membrane was sandwiched between the two PC parts, manually aligned and compressed at 130–140 °C and 150–200 p.s.i. for 8 h. After the bonding treatment, the chips were ready to use. A chip base and manifolds were designed using SolidWorks and fabricated in PC by micromachining.

The brain chip was made using the same procedure as the heart chip, but with the following additional steps. After 2 weeks of neural cell culture, the TOPAS (PolyLinks) substrates were assembled into the chip. The TOPAS was first deposited in the bottom of the base. Then, a PDMS gasket (moulded with an aperture corresponding to the neuronal growth area) was placed on top of the TOPAS substrate. The PC chip was finally placed on top of the gasket and the entire assembly was maintained on the base by screwing the manifolds to the base. Media reservoirs were fixed on one manifold. Reservoirs consisted of 5-ml syringes from which the top was cut. The plungers were cut and a biopsy punch used to create a minimal opening to the atmosphere. Connectors were fixed to the other manifold. The connector linked to the bottom channel (neuronal channel) was blocked and the connector linked to the upper channel was connected to a peristaltic pump (IPC series 16 channels, Ismatec). This configuration prevented

any shear stress on the neuronal constructs while enabling diffusion through the PC porous membrane.

The skin chip design reflects the requirement for a thicker tissue layer that needs to be uniformly strained. To accomplish this, the skin apical channel was a static oval reservoir with vertical posts around the perimeter. The posts enable collagen to gel around them, providing mechanical support for applying strain. The apical reservoir was open at the top to allow for deposition of viscous collagen and cells and resealable with a medical-grade adhesive film (Adhesives Research).

Mechanical actuation of chips. Microfluidic gut, lung and skin cultures were mechanically actuated using a programmable vacuum regulator system built in-house. The system consisted of a vacuum regulator (ITV0091–2BL, SMC) electronically controlled by an Arduino Leonardo and MAX517 digital-to-analog converter. The regulator outputs a sinusoidal vacuum profile with a user-settable amplitude and frequency.

Organ-chip culture. Organ chips were sterilized using oxygen plasma before applying an optimized extracellular matrix coating and subsequent seeding of epithelial and endothelial cells. Cell culture parameters are detailed in Supplementary Table 2. The chips were cultured until they reached a mature state specific to each organ type (Supplementary Figs. 7 and 8). Gut[36], liver[36,61], BBB[13], brain[13], heart[41] and kidney[36] chip cultures were performed as previously described. The lung chip was prepared as previously published[35], except that A549 alveolar epithelial cells (American Type Culture Collection (ATCC), CCL-185) and HUVECs (ATCC, PCS-100–010) were used. Only the vascular channels of each organ chip were seeded with endothelial cells and not in the connecting tubing or reservoirs.

Human skin chip. Before plating cells, the chips were surface-treated with oxygen plasma (Atto, Diener Electronic) at 30 mbar, 50 W for 2 min. The basal channel was then coated with a solution of 50 μg ml^{-1} human fibronectin (Corning, 354008) and 100 μg ml^{-1} bovine collagen I (Gibco, A10644-01) dissolved in cold DMEM supplemented with 1% penicillin–streptomycin (pen/strep). Additionally, an acellular collagen solution consisting of 5 mg ml^{-1} rat tail collagen was deposited on the apical membrane to help anchor the cell-laden gel to the PDMS membrane.

Human primary dermal fibroblasts derived from adult female forearm (ThermoFisher, C0135C) were cultured in DMEM-high glucose with Glutamax (ThermoFisher, 10569) supplemented with 10% fetal bovine serum. Cells were plated at 6,000 cells per cm^2 in standard cell culture flasks and used up to passage 7 for all experiments. Human primary neonatal epidermal keratinocytes derived from foreskin (ATCC, PCS-200–010) were cultured in keratinocyte growth medium (Dermal cell basal medium from ATCC, PCS-200–030) supplemented with a keratinocyte growth kit (ATCC, PCS-200–040). Cells were plated at 13,000 cells per cm^2 and used up to passage 5 for all experiments. Human dermal microvascular endothelial cells (HDMVECs; ATCC, PCS-110–010) were cultured in vascular Cell Basal Medium (ATCC, PCS-100–030) supplemented with an endothelial cell growth kit-VEGF (ATCC, PCS-100–041). Cells were plated at 1×10^4 cells per cm^2 in standard cell culture flasks and used up to passage 5 for all experiments.

Human adult fibroblasts were collected and resuspended at 1.5×10^6 cells per ml in dermal proliferation media (ThermoFisher, DMEM-high glucose supplemented with 1% pen/strep, 5% bovine calf serum (BCS) and 50 μg ml^{-1} sodium ascorbate). Dermal collagen solution (2.5 mg ml^{-1} bovine collagen I (Gibco, A10644-01) in 1× MEM; collagen was initially pH-adjusted by mixing with 5.5% v/v 1N NaOH before the addition of MEM) was combined with the fibroblast suspension to achieve a final density of 3×10^5 cells per ml in collagen gel; 90 μl of this cell–gel suspension was pipetted into the apical reservoir of each chip and cultured for 3 days. Human primary neonatal epidermal keratinocytes were collected and resuspended at 10.5×10^6 cells per ml in epidermal proliferation media (ThermoFisher; DMEM/F12 3:1, supplemented with 1% pen/strep, 0.3% chelated BCS, 50 μg ml^{-1} sodium ascorbate, 0.628 ng ml^{-1} progesterone and 10 ng ml^{-1} human recombinant epidermal growth factor). Dermal medium was aspirated from apical reservoirs and 25 μl of the human primary neonatal epidermal keratinocyte suspension was pipetted onto each fibroblast gel (2.6×10^5 keratinocytes per chip). Chips were incubated at 37 °C for 1 h to facilitate keratinocyte attachment. Chips were perfused with epidermal proliferation media for 4 days before switching to epidermal differentiation media (ThermoFisher; DMEM/F12 3:1, 1% pen/strep, 0.3% BCS, 50 μg ml^{-1} sodium ascorbate, 0.628 ng ml^{-1} progesterone, 265 μg ml^{-1} $CaCl_2$). An air–liquid interface was induced following 3 days of epidermal differentiation by aspirating the apical media and replacing the basal channel media with cornification media (ThermoFisher; DMEM/F12 1× 1% pen/strep, 2% BCS, 50 μg ml^{-1} sodium ascorbate and EGM-2 bullet kit (Lonza)) and maintained in the air–liquid interface for 3 weeks.

HDMVECs were seeded on the basal side of the chip on day 28 post initial fibroblast gel seeding. Cells were collected and resuspended in ATCC endothelial growth medium at a concentration of 5×10^6 cells per ml. Chip basal channels were recoated with fibronectin/collagen solution, incubated at 37 °C for 1 h and rinsed with 30 μl of warm ATCC endothelial growth medium. Skin chips were seeded with 25 μl of the HDMVEC suspension and incubated upside down for 2.5 h at 37 °C to allow for attachment of endothelial cells to the basal side of the chip membrane. Chips were then perfused with ATCC endothelial growth media overnight before switching back to cornification media.

Linked organ-chip perfusion. Each organ-chip module features a completely independent cell-free peristaltic perfusion system consisting of two inlet reservoirs, all tubing connections and two outlet reservoirs. Mature organ chips were loaded into Interrogator cartridges and connected to two inlet and two outlet reservoirs using Pharmed BPT tubing. The modules were perfused at a rate of 1 μl min^{-1} with flushing of the tubing at a rate of 5 μl min^{-1} every 4 h to maintain uniform perfusion rates during several weeks of culture.

Universal endothelial medium. Medium components were from Life Technologies unless otherwise stated. Universal endothelial medium comprised DMEM/F12 supplemented with EGM-2 Lonza bullet kit (Lonza), 0.5% fetal bovine serum, 1% pen/strep and growth factors (VEGF, EGF, IGF and FGFb) according to instructions provided with the kits.

Albumin ELISA. Media samples from inlet and outlet reservoirs of apical and basal channels of chips were sampled automatically as part of each fluidic linking cycle. Liver chip and kidney chip albumin concentrations were quantified using a human albumin ELISA quantitation kit (Bethyl Laboratories) per the manufacturer's protocol. Albumin production was normalized on a per cell basis, and reabsorption rates were calculated based on the difference between the inlet and outlet concentrations and elapsed times and media volumes, as previously described[61]. Rates were based on the difference between the inlet and outlet concentrations and elapsed times and media volumes.

Barrier function. Cascade Blue hydrazide, trisodium salt (Thermo Fisher Scientific) (for gut chip and skin chip), Dextran-Texas Red 3 kDa (for lung chip), Dextran-Texas Red 70 kDA (for BBB chip) and Dextran-Cascade Blue 10 kDa (Thermo Fisher Scientific) (for BBB chip and lung chip) and inulin-FITC 2–5 kDa (Sigma-Aldrich) were used as inert tracers in the medium to quantify organ-chip barrier function. The tracers were diluted to 100 μg ml^{-1} in apical media and flowed through the chip at 60 μl h^{-1} unless otherwise described. Media inputs and perfused medium outputs were collected for all channels and measured using a fluorescence plate reader set to the respective fluorophore excitation and emission filter sets. From these data, the P_{app} was calculated using equation (1)[24,62] as follows:

$$P_{app} = \frac{V_r \times V_d}{A \times t \times (V_r + V_d)} \times \ln\left(1 - \frac{C_{d\_out} \times (V_r + V_d)}{V_r \times C_r + V_d \times C_d}\right) \quad (1)$$

V_r is defined by the volume of receiving channel effluent after time t, C_r is the measured concentration of the tracer in the receiving channel effluent, t is time of effluent collection, A is the area of the main channel, V_d is defined by the volume of the dosing channel effluent after time t and C_{d_out} is the concentration of the dosing medium.

LDH assay. Media samples from inlet and outlet reservoirs of apical and basal channels of chips were sampled automatically as part of each fluidic linking cycle. LDH was measured using a CytoTox 96 non-radioactive cytotoxicity assay (Promega, G1780) per the manufacturer's protocol. The LDH concentration was quantified against the assay positive control diluted to a standard curve (0–3 μg ml^{-1}) in the respective organ-chip-specific media.

Morphology. Chips were rinsed in pre-warmed PBS and fixed in 4% paraformaldehyde (Sigma-Aldrich) for 10–20 min at room temperature. Immunocytochemistry was carried out after permeabilization in PBS with 0.05–0.1% Triton X-100 (Sigma-Aldrich) and blocking for 30 min in 3–5% BSA (Jackson ImmunoResearch) or 10% goat serum in PBS with 0.05–0.1% Triton-X 100. Primary antibodies were applied in 2% goat serum or 0.5% BSA overnight at 4 °C or at room temperature. The following primary antibodies were used for immunocytochemistry experiments: rabbit anti-GFAP (1:100; DAKO, Z-0334, lot no. 2002332); mouse anti-VE-cadherin (1:100; Abcam, ab166715); VE-cadherin (1:100; BD Biosciences, BD555661, lot no. 4324666); α-actinin (1:200; Abcam); mouse anti-ZO-1 (1:100; Invitrogen, 33-9100); anti-class III β-tubulin (1:200; Sigma-Aldrich); anti-neurofilament (1:100; Abcam); and anti-GFAP (1:200; Abcam). Cells were washed three times in PBS with 0.05–0.1% Triton-X 100 followed by staining with secondary antibody for 30–60 min at room temperature. The secondary antibodies were anti-rabbit or anti-mouse IgG conjugated with Alexa Fluor-488, Alexa Fluor-555 or Alexa Fluor-647 (Invitrogen). Hoechst (10 mg ml^{-1}, Life Technologies/Invitrogen, 33342) was used at a dilution of 1:5,000 for nuclei staining. For staining of F-actin, Alexa Fluor-488-phalloidin (A12379, lot no. 1583098) or Alexa Fluor-647-phalloidin (Life Sciences/Invitrogen) was used at a dilution of 1:30. For glass or TOPAS bottom samples, the substrate was removed from the dish and placed on a glass slide. ProLong Gold Antifade reagent (Molecular Probes Life Technologies) was added to preserve the samples, and glass coverslips were affixed using transparent nail polish. Prepared slides were either imaged immediately or stored at 4 °C. Imaging was carried out in a Zeiss 710 LSM

(Zeiss) or Olympus confocal microscope (Olympus) with appropriate filter cubes. Image processing was done using Fiji or Imaris (Bitplane, CHE).

Total protein. Lysate from the parenchymal cell channels was collected for total protein quantitation. Chips were rinsed with 1× PBS (−/−) and the basal channel was trypsinized to remove the endothelial cells. Next, RIPA buffer supplemented with 1× halt protease and phosphatase inhibitor single-use cocktail (Thermo Fisher Scientific) was added to the apical channel and incubated on ice for 20 min. Lysate was then collected from the chip and centrifuged at full speed for 10 min to remove insoluble components. Supernatant was removed and stored at −80 °C until the time of analysis. Total protein was determined using a Pierce BCA assay kit (Thermo Fisher Scientific) per the manufacturer's protocol.

Mass spectrometry. All chemicals were from Sigma unless otherwise noted. To prepare media samples and calibration samples for liquid chromatography–mass spectrometry (LC–MS) analysis, 20 µl of sample was mixed with 30 µl of an internal standards solution (10 µM D4-succinate in acetonitrile). After centrifugation at 18,000 × *g* for 10 min, 40 µl of supernatant was transferred to glass microinserts. All samples were kept at −80 °C until analysis.

LC–MS analyses were modified from a previously described method[63] and were performed on an Orbitrap Q-Exactive (Thermo Scientific) in line with an Ultimate 3000 LC (Thermo Scientific). The Exactive operated in the polarity-switching mode with positive voltage 3.0 kV and negative voltage 4.0 kV. Column hardware consisted of a Sequant ZIC-pHILIC column (2.1 × 50 mm, 5 µm, Millipore). The flow rate was 200 µl min^{-1}, and buffers consisted of acetonitrile 97% in water for buffer B, and 20 mm ammonium carbonate, 0.1% ammonium hydroxide in water for buffer A. The gradient ran from 100% to 40% buffer B for 20 min, then to 0% buffer B for 10 min. After maintaining buffer B at 0% for 5 min, it was ramped to 100% over 5 min and kept at 100% for 10 min. Metabolites were identified and quantified using the software Trace Finder and Compound Discoverer 2.0 (Thermo Scientific). Glutamine/glutamate standard curves were produced for quantifying these metabolites.

Passive tracer distribution analysis. Custom organ chips with PDMS membranes lacking pores were used to prevent any convective mixing between top and bottom channels. Chip medium was prepared by adding EGM-2 SingleQuot bullet kit (Lonza) to DMEM/F12 (Life Sciences). Inulin-FITC (Sigma Aldrich) fluorescent tracer was added to the inlet reservoirs at 100 µg ml^{-1}. For all transfers, 1-ml pipette tips were used (Neptune BT1000). Fluorescence was measured in black microplates (Corning, 3381 or Greiner, 655096) using a BioTek Synergy Neo plate reader with 485-nm excitation. Perfusion was enabled by connecting poreless membrane chips to the integrated peristaltic pump using 500 µm ID Pharmed BPT tubing (Thomas Scientific, 1203A38) and 19-gauge stainless steel connectors (straight from Microgroup and 90° elbow from Four Slide Products). Before assembly, all chips, tubing and fittings were sterilized with oxygen plasma and to make them hydrophilic, which prevents bubble formation at junctions.

Computational modelling of the behaviour of the system. All models were developed using CFDRC's Computational Biology (CoBi) tools[64]. For each organ chip, high-fidelity simulations of coupled fluid flow, biomechanics, mass transport, biochemistry and electrophysiology models were used to design specific organ geometry and operating parameters to reproduce the in vivo characteristics of the individual organs within the constraints of microfabrication and cell culture. Specifically, spatiotemporal MCRO models of the multiple compartments were established[36]. Tissues, the media channels and PDMS layers were represented with a coarse spatial computational mesh represented by control volumes parallel to the media flow and one control volume perpendicular to the direction of perfusion (PDMS, top channel, epithelial cell layer, membrane, endothelial cell layer, bottom channel, PDMS). This allowed us to solve general spatiotemporal transport equations related to accumulation, convection, diffusion and sources of inulin-FITC and other compounds.

The computational domain of these models replicates the entire in vitro organ, including microfluidic channels, PDMS membrane, epithelial and endothelial cellular barriers, package material (PDMS), inlet and outlet supply tubing, and reservoirs. For the organ chips described in this study, a coupled perfusing media flow and conjugate mass transfer model was applied to estimate the shear stress on cell barriers, species transport and mixing, trans-barrier transport and package material gas exchange. For organs with active mechanobiology, such as heart, gut or lung, coupled fluid–structures interaction models were used. For example, a computational model of the heart chip required 3D simulation of "muscular thin film" (MTF) structures[65] immersed in a medium and experiencing periodic mechanical contraction–relaxation movements (Supplementary Fig. 12; Supplementary Video 3). Supplementary Fig. 12 shows the detailed geometry of multiple MTFs in the heart chip device, where colour indicates the concentration of an adsorbed tracer compound on the MTF surface. Detailed geometries of the models used for liver, lung and skin organ chips are shown in Supplementary Figs. 10–12. Reduced-order differential equations were derived for all other organ chips to decrease computational time by integrating spatial terms for convection, diffusion and transport into individual fluxes across control volume boundaries. Solving the convective and diffusive terms in the microchannels was achieved with second-order accuracy in the direction parallel to media perfusion and analytically perpendicular to the direction of perfusion. This approach resolves spatial concentration gradients (for example, liver zonation and gut lumen path) and transit times.

Statistical analyses. Graphpad Prism was used to conduct all statistical tests and four-point logistic curve fitting for the interpolation of fluorescent tracer concentrations from standard curves. Unless otherwise noted, $P < 0.05$ values were considered significant, and mean and standard errors of the mean (s.e.m.) are shown in all plots.

Reporting Summary. Further information on research design is available in the Nature Research Reporting Summary linked to this article.

Data availability

All the data supporting the results in this study are available within the article and its Supplementary Information. Mass spectrometry data of brain-chip metabolites are available as Supplementary Dataset 1. The broad range of raw datasets acquired and analysed (or any subsets of it), which for reuse would require contextual metadata, are available from the corresponding author upon reasonable request.

Code availability

A SolidWorks CAD package of the Interrogator that defines all hardware components and assembly instructions are provided as Supplementary Design Files 1 and 2. The mass spectrometry data are provided as Supplementary Dataset 1. Control software is available at https://gitlab.com/wyss-microengineering/hydra-controller, and video tutorials are available at https://vimeo.com/album/5703210. Organ-chip simulations developed using CoBi Tools are available at http://medicalavatars.cfdrc.com/index.php/cobi-tools.

Received: 26 February 2019; Accepted: 25 November 2019;
Published online: 27 January 2020

References

1. Bhatia, S. N. & Ingber, D. E. Microfluidic organs-on-chips. *Nat. Biotechnol.* **32**, 760–772 (2014).
2. Lee, S. et al. Microfluidic-based vascularized microphysiological systems. *Lab Chip* **18**, 2686–2709 (2018).
3. Bhushan, A., Martucci, N. J., Usta, O. B. & Yarmush, M. L. New technologies in drug metabolism and toxicity screening: organ-to-organ interaction. *Expert Opin. Drug Metab. Toxicol.* **12**, 475–477 (2016).
4. Benigni, R. Predictive toxicology today: the transition from biological knowledge to practicable models. *Expert Opin. Drug Metab. Toxicol.* **12**, 989–992 (2016).
5. Mak, I. W., Evaniew, N. & Ghert, M. Lost in translation: animal models and clinical trials in cancer treatment. *Am. J. Transl. Res.* **6**, 114–118 (2014).
6. Ewart, L. et al. Application of microphysiological systems to enhance safety assessment in drug discovery. *Annu. Rev. Pharmacol. Toxicol.* **58**, 65–82 (2018).
7. Prantil-Baun, R. et al. Physiologically based pharmacokinetic and pharmacodynamic analysis enabled by microfluidically linked organs-on-chips. *Annu. Rev. Pharmacol. Toxicol.* **58**, 37–64 (2018).
8. Vernetti, L. et al. Functional coupling of human microphysiology systems: intestine, liver, kidney proximal tubule, blood–brain barrier and skeletal muscle. *Sci. Rep.* **7**, 42296 (2017).
9. Sung, J. H. et al. Using PBPK guided "Body-on-a-Chip" systems to predict mammalian response to drug and chemical exposure. *Exp. Biol. Med.* **239**, 1225–1239 (2014).
10. Wang, Y. I et al. Self-contained, low-cost Body-on-a-Chip systems for drug development. *Exp. Biol. Med.* **242**, 1701–1713 (2017).
11. Edington, C. D. et al. Interconnected microphysiological systems for quantitative biology and pharmacology studies. *Sci. Rep.* **8**, 4530 (2018).
12. Loskill, P., Marcus, S. G., Mathur, A., Reese, W. M. & Healy, K. E. µOrgano: a Lego®-like plug & play system for modular multi-organ-chips. *PLoS ONE* **10**, e0139587 (2015).
13. Maoz, B. M. et al. A linked organ-on-chip model of the human neurovascular unit reveals the metabolic coupling of endothelial and neuronal cells. *Nat. Biotechnol.* **36**, 865–874 (2018).
14. Coppeta, J. R. et al. A portable and reconfigurable multi-organ platform for drug development with onboard microfluidic flow control. *Lab Chip* **17**, 134–144 (2016).
15. Xiao, S. et al. A microfluidic culture model of the human reproductive tract and 28-day menstrual cycle. *Nat. Commun.* **8**, 14584 (2017).
16. Esch, M. B., Ueno, H., Applegate, D. R. & Shuler, M. L. Modular, pumpless body-on-a-chip platform for the co-culture of GI tract epithelium and 3D primary liver tissue. *Lab Chip* **16**, 2719–2729 (2016).

17. Oleaga, C et al. Multi-organ toxicity demonstration in a functional human in vitro system composed of four organs. *Sci. Rep.* **6**, 20030 (2016).
18. Sances, S. et al. Human iPSC-derived endothelial cells and microengineered organ-chip enhance neuronal development. *Stem Cell Rep.* **10**, 1222–1236 (2018).
19. Maschmeyer, I. et al. A four-organ-chip for interconnected long-term co-culture of human intestine, liver, skin and kidney equivalents. *Lab Chip* **15**, 2688–2699 (2015).
20. Bauer, S. et al. Functional coupling of human pancreatic islets and liver spheroids on-a-chip: towards a novel human ex vivo type 2 diabetes model. *Sci. Rep.* **7**, 14620 (2017).
21. Yu, F., Selva Kumar, N. D., Choudhury, D., Foo, L. C. & Ng, S. H. Microfluidic platforms for modeling biological barriers in the circulatory system. *Drug Discov. Today* **23**, 815–829 (2018).
22. Poisson, J. et al. Liver sinusoidal endothelial cells: physiology and role in liver diseases. *J. Hepatol.* **66**, 212–227 (2017).
23. Huh, D. et al. Microfabrication of human organs-on-chips. *Nat. Protoc.* **8**, 2135–2157 (2013).
24. Novak, R et al. Scalable fabrication of stretchable, dual channel, microfluidic organ chips. *J. Vis. Exp.* **140**, e58151 (2018).
25. Ewart, L. et al. Navigating tissue chips from development to dissemination: a pharmaceutical industry perspective. *Exp. Biol. Med.* **242**, 1579–1585 (2017).
26. Brown, J. A. et al. Recreating blood–brain barrier physiology and structure on chip: a novel neurovascular microfluidic bioreactor. *Biomicrofluidics* **9**, 054124 (2015).
27. Griep, L. M. et al. BBB on chip: microfluidic platform to mechanically and biochemically modulate blood–brain barrier function. *Biomed. Microdevices* **15**, 145–150 (2013).
28. Huh, D. et al. Reconstituting organ-level lung functions on a chip. *Science* **328**, 1662–1668 (2010).
29. Kim, H. J., Huh, D., Hamilton, G. & Ingber, D. E. Human gut-on-a-chip inhabited by microbial flora that experiences intestinal peristalsis-like motions and flow. *Lab Chip* **12**, 2165–2174 (2012).
30. Kim, H. J. & Ingber, D. E. Gut-on-a-Chip microenvironment induces human intestinal cells to undergo villus differentiation. *Integr. Biol.* **5**, 1130–1140 (2013).
31. Jang, K.-J. et al. Human kidney proximal tubule-on-a-chip for drug transport and nephrotoxicity assessment. *Integr. Biol.* **5**, 1119–1129 (2013).
32. Imura, Y., Asano, Y., Sato, K. & Yoshimura, E. A microfluidic system to evaluate intestinal absorption. *Anal. Sci.* **25**, 1403–1407 (2009).
33. Leclerc, E., Sakai, Y. & Fujii, T. Microfluidic PDMS (polydimethylsiloxane) bioreactor for large-scale culture of hepatocytes. *Biotechnol. Prog.* **20**, 750–755 (2004).
34. Kim, H. J., Li, H., Collins, J. J. & Ingber, D. E. Contributions of microbiome and mechanical deformation to intestinal bacterial overgrowth and inflammation in a human gut-on-a-chip. *Proc. Natl Acad. Sci. USA* **113**, E7–E15 (2016).
35. Huh, D. et al. A human disease model of drug toxicity-induced pulmonary edema in a lung-on-a-chip microdevice. *Sci. Transl Med.* **4**, 159ra147 (2012).
36. Herland, A. et al. Quantitative prediction of human drug pharmacokinetic responses enabled by fluidically coupled vascularized organ chips. *Nat. Biomed. Eng.* https://doi.org/10.1038/s41551-019-0498-9 (2020).
37. Toto, R. D. Conventional measurement of renal function utilizing serum creatinine, creatinine clearance, inulin and para-aminohippuric acid clearance. *Curr. Opin. Nephrol. Hypertens.* **4**, 505–509 (1995); discussion **4**, 503–504 (1995).
38. Rahn, K. H., Heidenreich, S. & Brückner, D. How to assess glomerular function and damage in humans. *J. Hypertens.* **17**, 309–317 (1999).
39. Rose, G. A. Measurement of glomerular filtration rate by inulin clearance without urine collection. *BMJ* **2**, 91–93 (1969).
40. Musah, S. et al. Mature induced-pluripotent-stem-cell-derived human podocytes reconstitute kidney glomerular-capillary-wall function on a chip. *Nat. Biomed. Eng.* **1**, 0069 (2017).
41. Kujala, V. J., Pasqualini, F. S., Goss, J. A., Nawroth, J. C. & Parker, K. K. Laminar ventricular myocardium on a microelectrode array-based chip. *J. Mater. Chem. B* **4**, 3534–3543 (2016).
42. Géraud, C. et al. Unique cell type-specific junctional complexes in vascular endothelium of human and rat liver sinusoids. *PLoS ONE* **7**, e34206 (2012).
43. Wikswo, J. P. et al. Scaling and systems biology for integrating multiple organs-on-a-chip. *Lab Chip* **13**, 3496–3511 (2013).
44. Low, L. A. & Tagle, D. A. Organs-on-chips: progress, challenges, and future directions. *Exp. Biol. Med.* **242**, 1573–1578 (2017).
45. Benam, K. H. et al. Small airway-on-a-chip enables analysis of human lung inflammation and drug responses in vitro. *Nat. Methods* **13**, 151–157 (2016).
46. Benam, K. H. et al. Matched-comparative modeling of normal and diseased human airway responses using a microengineered breathing lung chip. *Cell Syst.* **3**, 456–466.e4 (2016).
47. Bein, A. et al. Microfluidic organ-on-a-chip models of human intestine. *Cell. Mol. Gastroenterol. Hepatol.* **5**, 659–668 (2018).
48. Jalili-Firoozinezhad, S. et al. Modeling radiation injury-induced cell death and countermeasure drug responses in a human Gut-on-a-Chip. *Cell Death Dis.* **9**, 223 (2018).
49. Agarwal, A., Goss, J. A., Cho, A., McCain, M. L. & Parker, K. K. Microfluidic heart on a chip for higher throughput pharmacological studies. *Lab Chip* **13**, 3599–3608 (2013).
50. Hubatsch, I., Ragnarsson, E. G. E. & Artursson, P. Determination of drug permeability and prediction of drug absorption in Caco-2 monolayers. *Nat. Protoc.* **2**, 2111–2119 (2007).
51. Lehr, C.-M. *Cell Culture Models of Biological Barriers: In vitro Test Systems for Drug Absorption and Delivery* (CRC Press, 2003).
52. Roberts, M. S. & Rowland, M. A dispersion model of hepatic elimination. 1. Formulation of the model and bolus considerations. *J. Pharmacokinet. Biopharm.* **14**, 227–260 (1986).
53. Dong, J. & Park, M. S. Discussions on the hepatic well-stirred model: re-derivation from the dispersion model and re-analysis of the lidocaine data. *Eur. J. Pharm. Sci.* **124**, 46–60 (2018).
54. Somayaji, M. R., Das, D. & Przekwas, A. Computational approaches for modeling and analysis of human-on-chip systems for drug testing and characterization. *Drug Discov. Today* **21**, 1859–1862 (2016).
55. Robinson, D. E., Balter, N. J. & Schwartz, S. L. A physiologically based pharmacokinetic model for nicotine and cotinine in man. *J. Pharmacokinet. Biopharm.* **20**, 591–609 (1992).
56. Miller, P. G. & Shuler, M. L. Design and demonstration of a pumpless 14 compartment microphysiological system. *Biotechnol. Bioeng.* **113**, 2213–2227 (2016).
57. Jalili-Firoozinezhad, S et al. A complex human gut microbiome cultured in an anaerobic intestine-on-a-chip. *Nat. Biomed. Eng.* **3**, 520–531 (2019).
58. Phan, D. T. T. et al. A vascularized and perfused organ-on-a-chip platform for large-scale drug screening applications. *Lab Chip* **17**, 511–520 (2017).
59. Kasendra, M. et al. Development of a primary human Small Intestine-on-a-Chip using biopsy-derived organoids. *Sci. Rep.* **8**, 2871 (2018).
60. Benam, K. H. et al. Human lung small airway-on-a-chip protocol. *Methods Mol. Biol.* **1612**, 345–365 (2017).
61. Jang, K.-J. et al. Reproducing human and cross-species drug toxicities using a Liver-Chip. *Sci. Transl. Med.* **11**, eaax5516 (2019).
62. Tran, T. T. et al. Exact kinetic analysis of passive transport across a polarized confluent MDCK cell monolayer modeled as a single barrier. *J. Pharm. Sci.* **93**, 2108–2123 (2004).
63. Maddocks, O. D. K. et al. Serine starvation induces stress and p53-dependent metabolic remodelling in cancer cells. *Nature* **493**, 542–546 (2013).
64. Przekwas, A., Friend, T., Teixeira, R., Chen, Z. J. & Wilkerson, P. *Spatial Modeling Tools for Cell Biology* (CFD Research Corporation, 2006).
65. Wang, G. et al. Modeling the mitochondrial cardiomyopathy of Barth syndrome with iPSC and heart-on-chip technologies. *Nat. Med.* **20**, 616–623 (2014).

Acknowledgements

This research was sponsored by the Wyss Institute for Biologically Inspired Engineering at Harvard University and the Defense Advanced Research Projects Agency under Cooperative Agreement number W911NF-12-2-0036. The views and conclusions contained in this document are those of the authors and should not be interpreted as representing the official policies, either expressed or implied, of the Defense Advanced Research Projects Agency or the US government. This work was performed in part at the Center for Nanoscale Systems (CNS), a member of the National Nanotechnology Coordinated Infrastructure Network (NNCI), which is supported by the National Science Foundation under NSF award number 1541959. The CNS is part of Harvard University, the Harvard Materials Research Science and Engineering Center (DMR-1420570). The authors thank J. Caramanica and P. Machado for their machining expertise, M. Rosnach for his artwork, B. Fountaine and S. Kroll for their help with photography, M. Rousseau for help with videography, C. Vidoudez for mass spectrometry analysis, and J. Wikswo for helpful input at the start of this project.

Author contributions

R.N., A.H., B.M.M. and R.P.-B. led the data analyses for the generation of figures and, with D.E.I., prepared the manuscript. A.H., B.M.M., A. Chalkiadaki, D.B.C, M.C., T.H., M.B., S.D., E.A.F., S.S.F.J., T.G., S.J.-F., V.K., L.L., R.M., Y.M., J.A.N., B.O., T.-E.P., H.S., B.S., G.J.T., Z.T., T.H.-I., K.-J.J., A.S.-P. and M.Y. planned and performed biological experiments, with G.A.H., O.L., A.B., R.N., R.P.-B., K.K.P. and D.E.I. supervising the work. A.Cho., E.C., Y.C., J.F., R.F., C.F.N., R.N., G.A.H., J.A.G., N.W., K.K.P. and D.E.I. were responsible for the development and fabrication of the chip. J.S., G.T.II, C.H., J.F.-A., J.A.G. and D.L. conceptualized the robotics-based organ chip linking and developed early versions of the Interrogator instrument and software with an integrated robotic sampler. M.I., Y.C., S.M., A.D., T.D., T.F., O.H. B.A.N., and R.N were responsible for the software and hardware engineering and were involved in the development of the final instrument and sensors used in this study. D.D., M.R.S. and A.P. were responsible for MCRO model development and data analyses, working closely with A.H., B.M.M., R.P.-B. and R.N. Finally, R.N., R.P.-B., O.L., G.A.H., D.L., K.K.P. and D.E.I. were responsible for overseeing and orchestrating the entire effort.

Competing interests

D.E.I. is a founder and holds equity in Emulate, Inc., and chairs its scientific advisory board. K.K.P. is a consultant and a member of the scientific advisory board of Emulate, Inc. S.S.F.J., J.F.-A., G.A.H., C.H., K.-J.J., V.K., L.L., D.L., J.N., J.S., G.T.II and N.W. are employees of and hold equity in Emulate, Inc. A.B., Y.C., M.C., S.D., J.F.-A., T.F., E.A.F., J.A.G., G.A.H., T.H.-I., O.H., A.H., C.H., D.E.I., M.I., K.-J.J., V.K., L.L., D.L., O.L., B.M.M., Y.M., J.N., R.N., T.-E.P., K.K.P., J.S., A.S.-P., G.T.II and N.W. are inventors on intellectual property licensed to Emulate, Inc.

Additional information

Supplementary information is available for this paper at https://doi.org/10.1038/s41551-019-0497-x.

Correspondence and requests for materials should be addressed to D.E.I.

Reprints and permissions information is available at www.nature.com/reprints.

Publisher's note Springer Nature remains neutral with regard to jurisdictional claims in published maps and institutional affiliations.

nature research

Corresponding author(s): Don Ingber

Last updated by author(s): Sep 18, 2019

Reporting Summary

Nature Research wishes to improve the reproducibility of the work that we publish. This form provides structure for consistency and transparency in reporting. For further information on Nature Research policies, see Authors & Referees and the Editorial Policy Checklist.

Statistics

For all statistical analyses, confirm that the following items are present in the figure legend, table legend, main text, or Methods section.

n/a	Confirmed	
☐	☒	The exact sample size (*n*) for each experimental group/condition, given as a discrete number and unit of measurement
☐	☒	A statement on whether measurements were taken from distinct samples or whether the same sample was measured repeatedly
☐	☒	The statistical test(s) used AND whether they are one- or two-sided *Only common tests should be described solely by name; describe more complex techniques in the Methods section.*
☒	☐	A description of all covariates tested
☒	☐	A description of any assumptions or corrections, such as tests of normality and adjustment for multiple comparisons
☐	☒	A full description of the statistical parameters including central tendency (e.g. means) or other basic estimates (e.g. regression coefficient) AND variation (e.g. standard deviation) or associated estimates of uncertainty (e.g. confidence intervals)
☐	☒	For null hypothesis testing, the test statistic (e.g. *F*, *t*, *r*) with confidence intervals, effect sizes, degrees of freedom and *P* value noted *Give P values as exact values whenever suitable.*
☒	☐	For Bayesian analysis, information on the choice of priors and Markov chain Monte Carlo settings
☒	☐	For hierarchical and complex designs, identification of the appropriate level for tests and full reporting of outcomes
☒	☐	Estimates of effect sizes (e.g. Cohen's *d*, Pearson's *r*), indicating how they were calculated

Our web collection on statistics for biologists contains articles on many of the points above.

Software and code

Policy information about availability of computer code

Data collection	The custom operating code for the Interrogator was written in Javascript by using a suite of open-source packages and custom scripts. The code is available at https://gitlab.com/wyss-microengineering/hydra-controller The computational MCRO model for tracer distribution was developed using CFDRC's CoBi Tools, which are available for use at http://medicalavatars.cfdrc.com/index.php/cobi-tools
Data analysis	Graphpad Prism v7.0 and 8.0 were used for data analysis.

For manuscripts utilizing custom algorithms or software that are central to the research but not yet described in published literature, software must be made available to editors/reviewers. We strongly encourage code deposition in a community repository (e.g. GitHub). See the Nature Research guidelines for submitting code & software for further information.

Data

Policy information about availability of data

All manuscripts must include a data availability statement. This statement should provide the following information, where applicable:

- Accession codes, unique identifiers, or web links for publicly available datasets
- A list of figures that have associated raw data
- A description of any restrictions on data availability

All the data supporting the results in this study are available within the Article and its Supplementary Information. Mass-spectrometry data of brain-chip metabolites are available as Supplementary Dataset 1. The broad range of raw datasets acquired and analysed (or any subsets of it), which for reuse would require contextual metadata, are available from the corresponding author on reasonable request.

Field-specific reporting

Please select the one below that is the best fit for your research. If you are not sure, read the appropriate sections before making your selection.

☒ Life sciences ☐ Behavioural & social sciences ☐ Ecological, evolutionary & environmental sciences

For a reference copy of the document with all sections, see nature.com/documents/nr-reporting-summary-flat.pdf

Life sciences study design

All studies must disclose on these points even when the disclosure is negative.

Sample size	Studies of organ-chip linking were performed with two replicates (n = 2). Unlinked chips (n > 4) were cultured in parallel without fluidic linkage to act as additional controls.
Data exclusions	Studies experiencing failure owing to instrumentation errors or organ-chip contamination were not included in the reported data. Instrumentation error occurred multiple times during early development, but was eliminated by the time the fully linked studies were conducted. Contamination of specific chips occurred rarely and during early development. A description of the failure modes is provided in the manuscript.
Replication	Replication was assessed in detail for the instrumentation. We observed the results of pipetting and fluid perfusion to be more repeatable than manual handling in all cases. This was further assessed by using the computational MCRO model, because automated handling resulted in greater correlations with model predictions than data manually acquired during initial development.
Randomization	At least 8 organ chips were prepared for each organ type, and randomly selected for each instrument. The rest of the chips were used as parallel controls.
Blinding	Blinding was not feasible during the execution of this study.

Reporting for specific materials, systems and methods

We require information from authors about some types of materials, experimental systems and methods used in many studies. Here, indicate whether each material, system or method listed is relevant to your study. If you are not sure if a list item applies to your research, read the appropriate section before selecting a response.

Materials & experimental systems

n/a	Involved in the study
☐	☒ Antibodies
☐	☒ Eukaryotic cell lines
☒	☐ Palaeontology
☒	☐ Animals and other organisms
☒	☐ Human research participants
☒	☐ Clinical data

Methods

n/a	Involved in the study
☒	☐ ChIP-seq
☒	☐ Flow cytometry
☒	☐ MRI-based neuroimaging

Antibodies

Antibodies used	The following primary antibodies were used for immunocytochemistry experiments: rabbit anti-glial fibrillary acidic protein (GFAP) (DAKO, 1:100, Z-0334, Lot #2002332), mouse anti-vascular endothelial (VE)-cadherin (Abcam, ab166715, Cambridge, MA, USA 1:100), (VE)-cadherin (BD Biosciences, USA 1:100, BD555661, Lot #4324666), alpha-actinin (Abcam, Cambridge, UK, 1:200), mouse anti-zona occludens-1 (ZO-1) (Invitrogen 1:100, Cat #33-9100), anti-βIII-tubulin (Sigma-Aldrich, 1:200), anti-neurofilament (Abcam, Cambridge, MA, USA 1:100), anti-glial fibrillary acidic protein (GFAP, Abcam, Cambridge, MA, USA, 1:200). Cells were washed three times in phosphate-buffered saline with 0.05 to 0.1 % Triton-X 100, followed by staining with secondary antibody staining for 30 to 60 min at RT. The secondary antibodies were anti-rabbit or anti-mouse IgG conjugated with Alexa Fluor-488, Alexa Fluor-555, or Alexa Fluor-647 (Invitrogen, Carlsbad, CA, USA). Hoechst (10 mg/mL, 33342, Life Technologies/Invitrogen, Carlsbad, CA, USA) was used at a dilution of 1:5000 for nuclei staining. For staining of F-actin, Alexa Fluor-488-phalloidin (A12379, Lot #1583098) or Alexa Fluor-647-phalloidin (Life Sciences/Invitrogen, Carlsbad, CA, USA) were used at dilution of 1:30.
Validation	Antibodies were largely used without validation beyond the information available from the vendors, and results were examined for morphological accuracy.

Eukaryotic cell lines

Policy information about cell lines

Cell line source(s)	CaCo2-BBe1 colon cancer cells (ATCC CRL-2102), A549 alveolar epithelial cells (ATCC CCL-185), and human umbilical vein endothelial cells (ATCC PCS-100-010).
Authentication	No authentication of the cell lines was performed other than morphological assessment.
Mycoplasma contamination	Cell lines were regularly screened for mycoplasma contamination.
Commonly misidentified lines (See ICLAC register)	No commonly misidentifies cell lines were used.